CHAPTER TWO

Minor Groove-Binding Intercalator Conjugates

The text of this chapter was taken in part from a manuscript co-authored with Professor Peter B. Dervan (Caltech).

Fechter EJ, Dervan PB; Allosteric Inhibition of Protein-DNA Complexes by Polyamide-Intercalator Conjugates, *J. Am. Chem. Soc.* **2003**, 125, 8476-8485.

Abstract

The sequence-specific inhibition of essential protein-DNA contacts in the promoter of a gene is a central issue for the regulation of gene expression by chemical methods. Hairpin polyamides have been shown to inhibit protein-DNA complexes in some but not all cases. For example, polyamides co-occupy the same DNA sequence in the minor groove in the presence of major-groove binding bZip proteins. Hairpin polyamide-acridine conjugates were synthesized and shown to bind the minor groove of DNA with high affinity in a sequence-specific manner. The polyamide-acridine conjugates were shown to unwind DNA (ϕ = 14-15^{o}) –evidence for intercalation by the acridine moiety. Importantly, the polyamide-intercalator conjugates, which combine sequence-specific groove binding with proximal local unwinding, inhibit major-groove DNA binding by the GCN4 bZip protein and an Sp1/Sp3:DNA complex. Additionally, several polyamide-acridine conjugates can localize to the nucleus of cells. This class of DNA binding molecules creates a sequence-specific allosteric change in DNA structure and has the potential to be a general inhibitor of transcription factor binding independent of the specific protein-DNA structure.

Introduction

Controlling gene expression with DNA binding small molecules is a challenge at the interface of chemistry and biology.[1-4] Toward this goal, a crucial step is to inhibit essential transcription factors from binding specific DNA elements in the promoter of a gene.[5,6] During the past decade, the X-ray and NMR structures of a large number of protein-DNA complexes have been reported.[7-16] There are distinct families of protein motifs which are recurring themes in DNA complexes, such as zinc fingers,[9] bZip,[10,11] and winged helix-turn-helix.[12] In a formal sense, there are at least two mechanisms by which synthetic ligands might compete with specific protein-DNA binding: direct steric interference or an allosteric alteration of DNA structure or some combination of both. One strategy is to consider each family of protein-DNA complexes as a unique target and, from a consideration of the complex structure, arrive at a protein-specific strategy for inhibition by a polyamide binding in the minor groove.[17-25] In the simplest case, a minor-groove binding protein would be inhibited by a minor-groove binding polyamide for reasons of steric blockade.[17-20] A major-groove/minor-groove binding protein also would be inhibited by judicious placement of the polyamide near crucial protein minor-groove contacts.[18] A major-groove protein that distorts DNA from a B-form helix, either by bending or alteration of groove width, might not be compatible with a minor-groove polyamide that prefers B-form. Indeed, recent studies have documented that pyrrole-imidazole polyamides, which bind sequence-specifically in the minor groove of DNA, are able to block several different classes of eukaryotic transcription factors (TFs) from binding their cognate DNA sites.[17-25] For example, the general transcription factor TATA box-binding protein (TBP) and the lymphoid enhancer factor (LEF-1) can be inhibited by

steric interference with minor-groove contacts as well as by "locking" the DNA into a B-type conformation upon polyamide binding.[18] Allosteric inhibition may also extend to a class of major-groove binding TFs that recognize sites containing narrow minor grooves, such as the NF-κB heterodimer, by widening the minor groove upon polyamide binding.[23] Proteins recognizing specific sequences in the major groove with additional contacts to phosphates outside the groove, such as the winged-helix-turn-helix TF (Ets-1)[12] and the basic helix-loop-helix (bHLH),[16] provide another means of inhibition through phosphate interference by polyamides.[24,25] However, some essential DNA binding proteins remain resistant to inhibition by polyamide binding. For example, minor-groove binding polyamides can co-occupy binding sites of major-groove binding proteins such as the bZip class.[26] Presumably, polyamide contacts are confined to the minor groove[28,29] and the protein is confined to the major groove[10,11] with negligible DNA structural changes induced by either ligand.[28,29] One successful bZip-specific strategy was the design of polyamides containing an Arg-Pro-Arg positive patch which competes with protein side chains for electrostatic phosphate contacts on the DNA backbone.[30-32] Nonetheless, Arg-Pro-Arg-polyamides are limited to targeting phosphate contacts and are not likely to significantly disrupt the DNA topology of TF binding sites. A summary of transcription factors inhibited by sequence-specific polyamides is provided in Table 2.1. The importance of major-groove contacts in TF-DNA complexes provides an impetus for the development of a general class of polyamides that can selectively inhibit any DNA protein complex.

Numerous TF binding sites in the promoters of key genes lack structural information regarding the protein-DNA complex. This underlines the need to find a

Table 2.1 Transcription factor inhibition by polyamides.

Transcription Factor	DNA-Binding Motif	Groove Recognition	Proposed Mechanism of Inhibition	Gene Target
TBP/TFIID	Saddle	minor	allosteric	mRNA-coding genes
LEF-1	HMG box	minor	allosteric	HIV-1
TFIIIB	N/A	minor	steric	tRNA genes
IE-86	minor	minor	steric	CMV MIEP
Tax	N/A	minor	steric	HTLV-1
TFIIIA	Cys_2His_2ZnF	minor/Major	steric	5S ribosomal RNA
NFκB	Rel homology domain	Major	allosteric	mRNA-coding genes/viral gene expression
Zif 268	Cys_2His_2ZnF	Major	allosteric	mRNA-coding genes
Ets-1	winged-helix-turn-helix	Major	phosphate interference	HIV-1
Dpn	basic helix-loop-helix	Major	phosphate interference	*Drosophila* neural genes
GCN4	bZip	Major	phosphate interference	yeast mRNA-coding genes

general solution for polyamide design that will inhibit the binding of any TF regardless of knowledge of the protein-DNA structure. One possible solution is a sequence-specific bifunctional molecule that distorts the DNA helix upon binding. The sequence-specific alteration of DNA structure would disrupt essential protein-DNA contacts. One such class of molecules would be a minor groove-binding intercalator hybrid with the specificity of a polyamide for DNA recognition and the ability to alter DNA structure by intercalator-induced local unwinding and helix extension (Figure 2.1). The insertion of flat intercalators between adjacent base pairs of the double helix causes a 3.4 Å extension and a 10-26^{o} unwinding, depending on the aromatic moiety.[33-36] This localized distortion is usually confined to within a few base pairs of the intercalation site and shows little dependence on DNA sequence.[33-37]

A key design issue is whether the groove binding hairpin polyamide can retain its capacity for sequence discrimination when covalently linked to an intercalator (Figures 2.1 and 2.2). An effective design of sequence-specific DNA intercalation by polyamide-

intercalator conjugates requires the polyamide to associate with high affinity and selectivity with compatible intercalation at a proximal DNA site. The covalent linkage between the two moieties should freely accommodate both modes of binding. The selected intercalator must provide sufficient DNA unwinding to disrupt TF contacts without disrupting the array of hydrogen bonds necessary for high polyamide-DNA association and specificity.

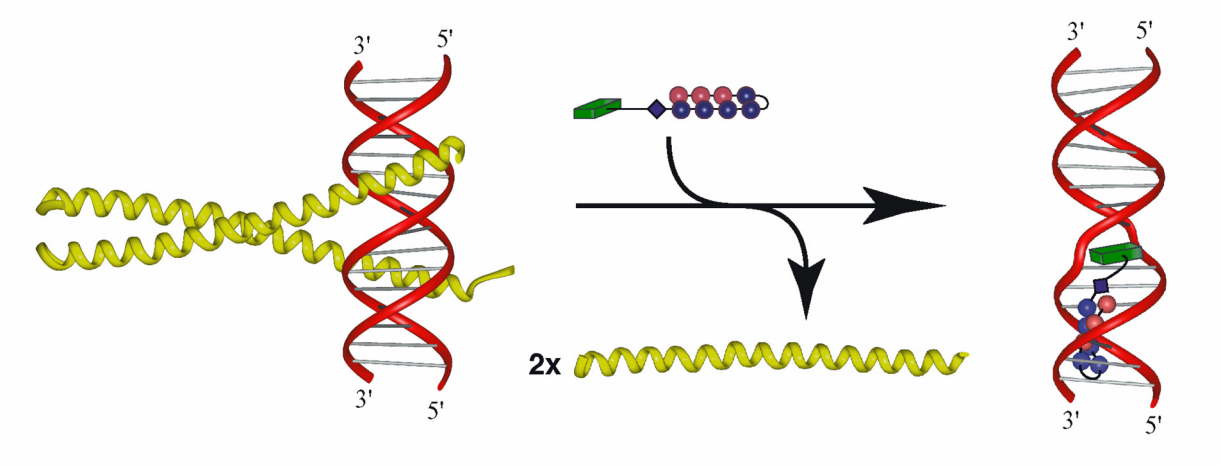

Figure 2.1 Model for allosteric inhibition of a protein-DNA complex by a polyamide-intercalator conjugate. The GCN4 homodimer (yellow) is displaced by the intercalating moiety (green) of the polyamide conjugate. Blue and red spheres represent pyrrole and imidazole amino acids, respectively. The blue diamond represents *β*-alanine.

We report here the synthesis of four polyamide-acridine conjugates **1-4** and their abilities to selectively inhibit the major-groove binding bZip transcription factor GCN4. Polyamides were covalently linked to a 9-chloroacridine or *N*-(2-(dimethylamino)ethyl)-9-chloroacridine-4-carboxamide with one of two poly(ethylene glycol) (PEG) linkers (Figure 2.3). The class of acridine intercalators was chosen for its relatively modest degree of unwinding (15-17°),[37,38] preference for intercalation via the minor groove, and favorable cellular uptake properties which could be important in cell culture applications.[38-40] Within this class, *N*-(2-(dimethylamino)ethyl)acridine-4-carboxamide (DACA) and its derivatives are classified as "threading" intercalators given that the

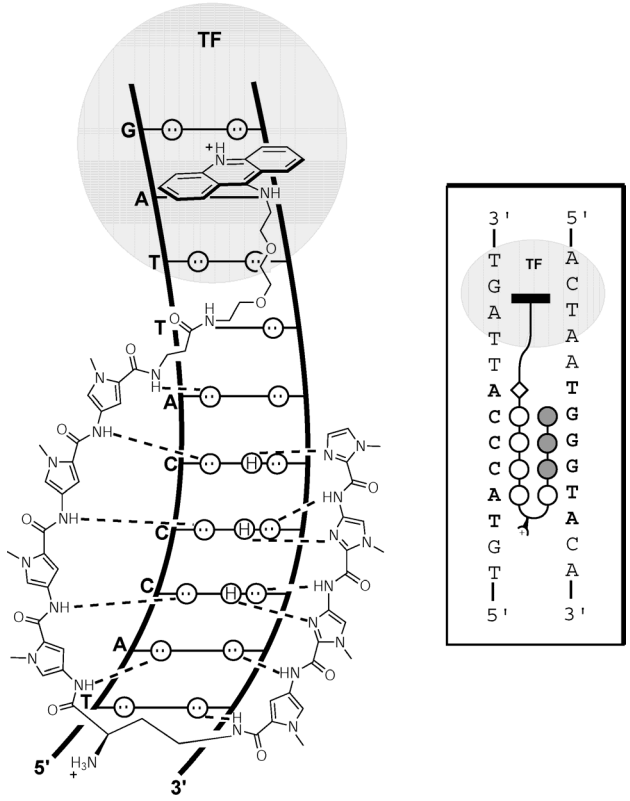

Figure 2.2 (Left) Hydrogen-bonding model of the eight ring hairpin polyamide conjugate ImImImPy-(*R*)^{H2N}γ-PyPyPyPy-*β*-Do-Acr bound to the minor groove of 5'-TACCCAT-3'. Circles with dots represent lone pairs of N3 of purines and O2 of pyrimidines. Circles containing an H represent the N2 hydrogens of guanine. Putative hydrogen bonds are illustrated by dotted lines. The large shaded circle represents the GCN4 transcription factor (TF). (Right) Ball and stick model of the polyamide-conjugate binding its target site (bold) adjacent to the binding of the protein GCN4. Filled circles denote imidazole, open circles represent pyrrole, and the diamond represents *β*-alanine. The shaded bar depicts the acridine intercalator.

cationic carboxamide side chain, *peri* to the heterocyclic nitrogen, has been shown to sterically block regions of the major groove, providing greater potential for TF complex inhibition.[40-42] The DNA binding affinity and specificity of each conjugate, as well as analogs lacking the acridine unit, were evaluated using quantitative DNase I footprinting. Binding site size was measured using methidiumpropyl-EDTA (MPE) footprinting. Intercalation unwinding angles were determined using closed-circular DNA (ccDNA) methods developed by Crothers and Zeman.[43,44] An electrophoretic mobility shift assay (EMSA) using the carboxy-terminal 60 amino acids (222-281) of the GCN4

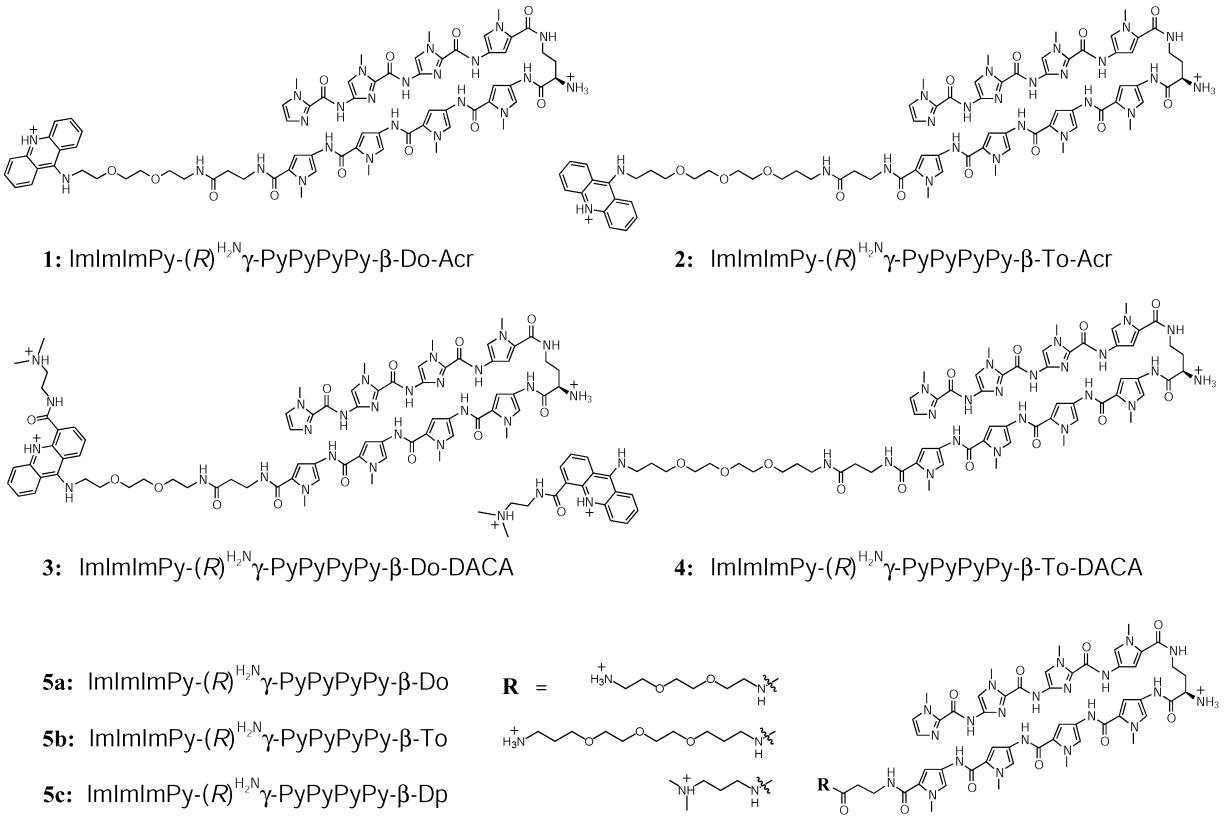

Figure 2.3 Structures of the hairpin polyamide-acridine conjugates. Do represents 2,2'-(ethylenedioxy)-bis(ethylamine), and To represents 4,7,10-trioxa-1,13-tridecanediamine.

leucine zipper dimerization domain as well as the Sp1/Sp3 transcription factor was used to evaluate inhibition of protein-DNA binding. The conjugates were also evaluated for inhibition of topoisomerase II. Finally, various analogs to the first series of conjugates were synthesized and those containing fluorescent properties were assessed for cellular uptake.

Results

Synthesis of Polyamide-Acridine Conjugates 1-4

Eight-ring hairpin polyamide conjugates containing the sequence ImImImPy-$(R)^{\text{NHFmoc}}\gamma$-PyPyPyPy-$\beta$-Pam-resin were synthesized in a stepwise manner on Boc-β-

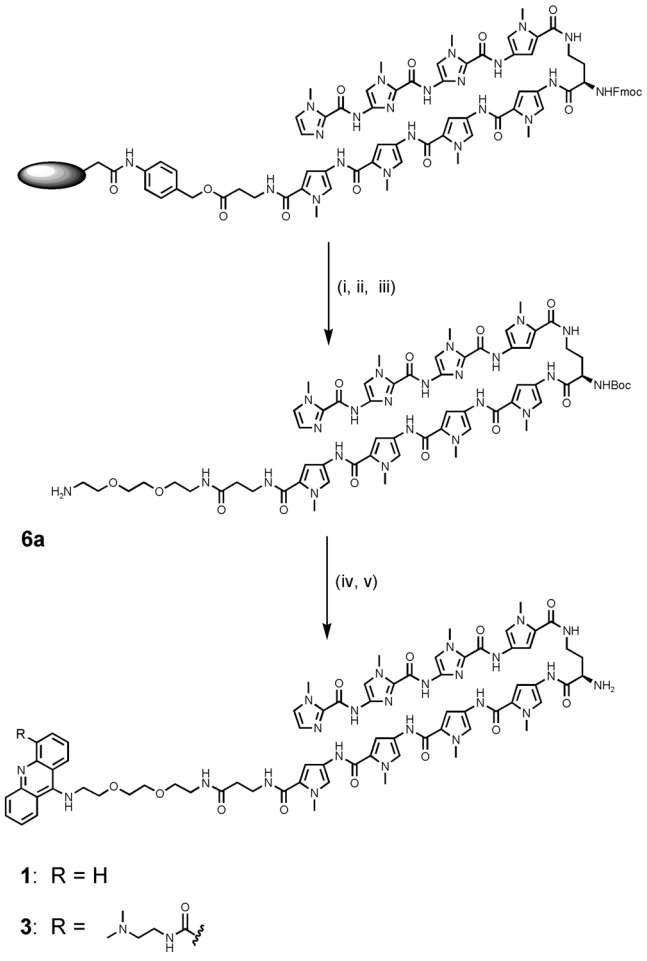

Figure 2.4 Synthetic scheme for polyamide-acridine conjugates: (i) 4:1 piperidine-DMF, 25 °C (30 min); (ii) Boc_2O, DIEA, NMP, 55 °C (30 min); (iii) 2,2'-(ethylenedioxy)-bis(ethylamine), 55 °C (18 h); (iv) 9-chloroacridine or *N*-(2-(dimethylamino)ethyl)-9-chloroacridine-4-carboxamide, phenol, DIEA, 100 °C (1 h); (v) 80% TFA/DCM, 0.4 M PhSH, 25 °C (15 min).

alanine Pam resin using established Boc-chemistry protocols.[45] The Fmoc-protected diaminobutyric acid (DABA) "turn" monomer was then deprotected by treatment with piperidine followed by reprotection with Boc_2O prior to polyamide aminolytic cleavage using one of two diamine linking agents (Figure 2.4). After reverse-phase HPLC purification, the polyamide primary amine was allowed to react with 9-chloroacridine derivatives in phenol at elevated temperature in the presence of diisopropylethylamine

(DIEA). The crude material was then deprotected with trifluoroacetic acid (TFA) and the desired conjugate was purified by preparatory reverse phase HPLC.

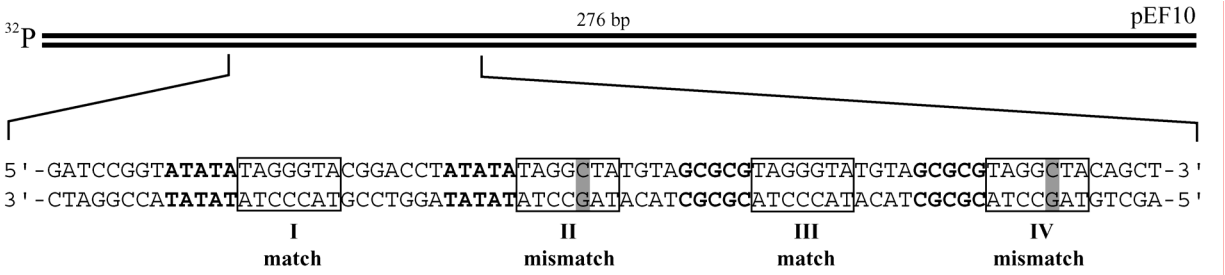

Figure 2.5 Sequence of the synthesized insert from the pEF10 plasmid containing two 7-bp target match sites (**I** and **III**) and two single bp mismatch sites (**II** and **IV**). Target sites are shown in boxes and mismatch sites are shaded.

Binding Energetics and Sequence Specificity

Quantitative DNase I footprint titrations were performed on a 5'-^{32}P-labeled PCR-amplified fragment of pEF10 (Figure 2.5) to determine the equilibrium association constants (K_a) of polyamides **1-4** (Table 2.2). The amplified fragment contains two

Table 2.2 Equilibrium Association Constants (M^{-1})[a]

polyamide	site I 5'-*ATATA*TAGGG TA-3'	site II 5'-*ATATA*TAGG**C** TA-3'	site III 5'-*GCGCG*TAGGG TA-3'	site IV 5'-*GCGCG*TAGG**C** TA-3'
1	1.8 (±0.2) × 10^{10}	4.1 (±0.5) × 10^{9}	1.4 (±0.2) × 10^{10}	1.8 (±0.1) × 10^{9}
2	1.4 (±0.1) × 10^{10}	1.5 (±0.2) × 10^{9}	8.9 (±0.8) × 10^{9}	5.8 (±0.8) × 10^{8}
3	7.5 (±0.6) × 10^{9}	1.0 (±0.1) × 10^{9}	9.5 (±0.9) × 10^{9}	1.1 (±0.1) × 10^{9}
4	7.1 (±0.5) × 10^{9}	8.8 (±1.0) × 10^{8}	1.3 (±0.1) × 10^{10}	1.5 (±0.1) × 10^{9}
5a	3.8 (±0.7) × 10^{9}	4.2 (±0.5) × 10^{8}	3.3 (±0.4) × 10^{9}	1.4 (±0.1) × 10^{8}
5b	4.5 (±0.4) × 10^{9}	4.8 (±0.4) × 10^{8}	3.5 (±0.3) × 10^{9}	1.1 (±0.2) × 10^{8}
5c	1.1 (±0.1) × 10^{10}	1.1 (±0.2) × 10^{9}	8.7 (±1.3) × 10^{9}	4.2 (±0.6) × 10^{8}

[a] The reported association constants are the average values obtained from three DNase I footprint titration experiments. The standard deviation for each data set is indicated in parentheses. The flanking intercalation sites are indicated in italics and the mismatch sites are shown in bold. Assays were performed at 22°C at pH 7.0 in the presence of 10 mM Tris·HCl, 10 mM KCl, 10 mM $MgCl_2$, and 5 mM $CaCl_2$.

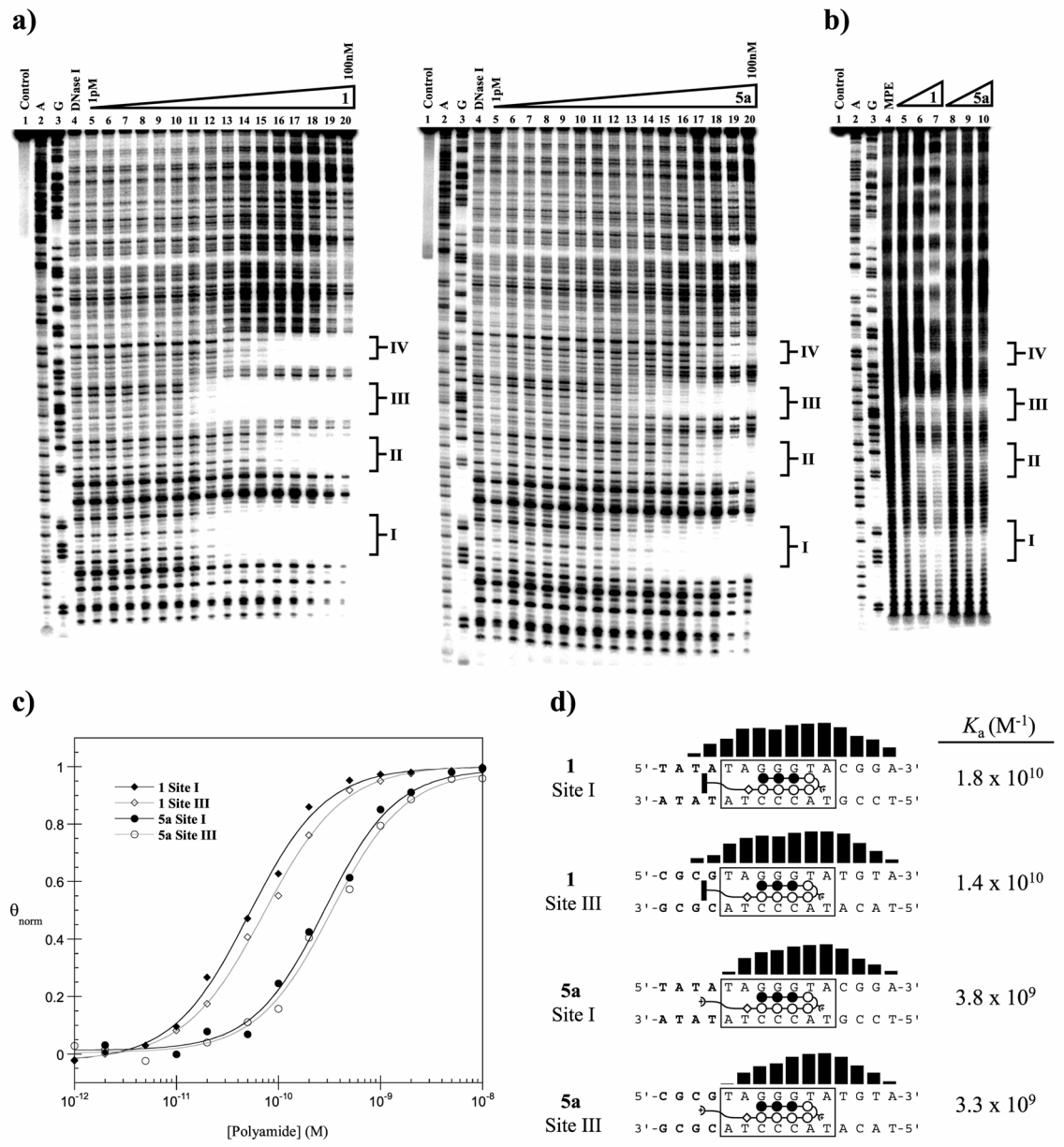

Figure 2.6 (a) Quantitative DNase I footprint titration experiments with ImImImPy-(R)^{H2N}*γ*-PyPyPyPy-*β*-Do-Acr (**1**) and ImImImPy-(R)^{H2N}*γ*-PyPyPyPy-*β*-Do (**5a**) on the PCR-amplified 5'-^{32}P-labeled 276-bp fragment of pEF10. **I**, **II**, **III**, and **IV** correspond to the sites indicated in Figure 2.5: Lane 1, intact DNA; lane 2, A reaction; lane 3, G reaction; lane 4, DNase I standard; lanes 5, 6, 7, 8, 9, 10, 11, 12, 13, 14, 15, 16, 17, 18, 19, and 20, 1 pM, 2 pM, 5 pM, 10 pM, 20 pM, 50 pM, 100 pM, 200 pM, 500 pM, 1 nM, 2 nM, 5 nM, 10 nM, 20 nM, 50 nM, 100 nM polyamide, respectively. All reactions contain 15 kcpm amplified fragment, 10 mM Tris·HCl (pH 7.0), 10 mM KCl, 10 mM $MgCl_2$, and 5 mM $CaCl_2$. Data were obtained for the binding sites indicated to the right of the gel. (b) MPE·Fe^{II} footprinting of **1** and **5a**: Lane 1, intact DNA; lane 2, A reaction; lane 3, G reaction; lane 4, MPE·Fe^{II} standard; lanes 5, 6, and 7, 200 pM, 2 nM, and 20 nM **1**; lanes 8, 9, and 10, 200 pM, 2 nM, and 20 nM **5a**. (c) Binding isotherms at match sites for **1** and **5a**. θ_{norm} points were obtained using storage phosphor autoradiography and processed by standard methods. Each data point shows the average value obtained from three footprinting experiments. The solid curves are best-fit Langmuir binding titration isotherms obtained from nonlinear least squares algorithm. (d) MPE·Fe^{II} protection patterns at 2 nM concentration for each match site. Bar heights are proportional to the relative protection from cleavage at each band. K_a values of the corresponding match sites are shown to the right.

polyamide match sites 5'-TAGGGTA-3' (**I** and **III**) and two polyamide mismatch sites 5'-TAGG**C**TA-3' (**II** and **IV**). Each site contains either an upstream AT-rich (**I** and **II**) or GC-rich (**III** and **IV**) flanking sequence to evaluate the significance of the intercalation site composition on conjugate binding. The control compound **5c** contains a C-terminal *N*,*N*-dimethylaminopropylamine (Dp) monomer and was used as a baseline for comparing binding energetics (K_a = 1.1 × 10^{10} M^{-1} and 8.7 × 10^9 M^{-1} for sites **I** and **III**, respectively). Replacing the Dp residue with PEG-linked primary amines (polyamides **5a** and **5b**) results in a decreased binding affinity at both match sites (K_a = 3.8 × 10^9 M^{-1} and 4.5 × 10^9 M^{-1} for site **I**, respectively, and K_a = 3.3 × 10^9 M^{-1} and 3.5 × 10^9 M^{-1} for site **III**, respectively). However, the addition of either acridine intercalator to either PEG linker (**1-4**) recovers the lost binding affinity at both match sites (example shown in Figure 2.6). Acridine conjugates **1** and **2**, containing both short and long PEG linkers, respectively, bound to the AT flanked match site (**I**) with the highest affinities (K_a = 1.8 × 10^{10} M^{-1} and 1.4 × 10^{10} M^{-1}, respectively). Each showed a slight preference (~1.5-fold) for the AT-flanked match sequence (**I**) over the GC match sequence (**III**). The specificity over mismatch sites was maintained for compound **2** and slightly decreased for the shorter linked compound **1**. The DACA-containing counterparts, conjugates **3** and **4**, showed slightly lower affinities (K_a = 7.5 × 10^9 M^{-1} and 7.1 × 10^9 M^{-1}, respectively) for the AT-flanked match site (**I**) but a slight preference (~1.5-fold) for the GC-flanked match site (**III**) (K_a = 9.5 × 10^9 M^{-1} and 1.3 × 10^{10} M^{-1}, respectively). The specificity over mismatch sites was again maintained for the longer linked compound **4** and slightly decreased for the shorter linked compound **3**.

These results show that polyamide-acridine conjugates are capable of maintaining the binding affinity and sequence specificity when compared to the parent hairpins. The loss of affinity by replacement of the C-terminal Dp monomer with a PEG linker (**5a** and **5b**) is consistent with studies in our group. The recovery of affinity upon the addition of an acridine intercalator to the PEG linker (without changing the net cationic charge in the cases of **1** and **2**) suggests that the acridine moiety participates in DNA binding. The binding affinity of polyamide-acridine conjugate **1** is $K_a = 1.8 \times 10^{10}$ M^{-1}, a 5-fold increase over the parent polyamide **5a**, $K_a = 3.8 \times 10^9$ M^{-1}. From previous work, the affinity of 9-aminoacridine can be estimated to be $K_a \sim 7 \times 10^4$ M^{-1}.[24] Since the energetic gain for the linked acridine is modest, a factor of 5-fold rather than 10^5, i.e., $K_a^{conjugate} < (K_a^{polyamide}) \times (K_a^{acridine})$, we conclude there is a negative cooperative association of the combined ligands to DNA. Additionally, the modest preference for GC flanking sequences by **3** and **4** is consistent with the previously reported binding affinities of DACA and its derivatives.[41,42] As with unconjugated DACA, compounds **3** and **4** may allow the carboxamide side chain to reside in the major groove and become stabilized by a specific hydrogen bond between the $-NMe_2H^+$ group to the N7 of guanine, leading to the modest GC binding preference.[40] The increased affinity from the side chain association may be slightly offset by an unfavorable steric interaction of the PEG linker with the exocyclic NH_2 in the minor groove of guanine-rich sequences. This steric effect should exist for the compounds lacking the carboxamide side chain **1** and **2** and may account for the slight preference for AT flanking sequences.

The sequence specificity of the conjugates with longer linkers **2** and **4** was maintained while that of the conjugates with shorter linkers **1** and **3** showed a slight

decrease. This result suggests that the trioxa-diamine linker (To) was sufficiently long to permit mutual minor-groove and intercalative binding without interrupting the hydrogen bonds essential for high polyamide association and specificity. The shorter dioxa-diamine linker (Do) may direct the intercalator nearer the polyamide, preventing optimal mutual binding and dislocating key recognition elements.

Binding Site Size

Additional support for intercalative binding of conjugates **1-4** is provided by methidiumpropyl-EDTA (MPE) footprinting, wherein the binding site size can be determined at much higher resolution than by DNase I methods. MPE footprints (Figure 2.6b) confirm that conjugates **1-4** bind to the designed 7-bp match sites **I** and **III**. Binding to the mismatch sites **II** and **IV** is only observed at significantly higher polyamide concentrations. Protection patterns for conjugates **1-4** (Figure 2.6d) reveal increases in binding site size by two base pairs compared to nonconjugated controls **5a** and **5b**. The saturation intercalation conditions of MPE footprinting result in at least every other potential methidium intercalation site unoccupied (neighbor exclusion). The intercalation of conjugates **1-4** would therefore prevent intercalation of methidium at the site adjacent to the polyamide N-terminus (albeit not the case if strictly groove binding) and in turn prevent strand cleavage at this site. The nearest possible location for strand cleavage using the intercalative model of **1-4** would be two base pairs past the N-terminus of the control polyamide (Figure 2.6b).

Helical Unwinding Angle Determination

To confirm intercalation and quantitatively measure the unwinding effects of the polyamide conjugates, compounds **1** and **4** were selected for helical unwinding assays using closed-circular pUC19 DNA.[43,44] Relaxation reactions were carried out on pUC19 preequilibrated with varying concentrations of polyamides[46] or pUC19 alone. Following topoisomerase I (Topo I) treatment and extraction of intercalated conjugate, the two-dimensional (2D) agarose gel electrophoresis of ccDNA for all reactions containing conjugates **1** and **4** resulted in a primarily negative distribution of topoisomers (Figure 2.7a, left). Control experiments lacking polyamides resulted in a primarily positive distribution of topoisomers (Figure 2.7a, right). Mathematical treatment of the difference in the most abundant topoisomers between control and polyamide-acridine conjugate reactions showed decreasing apparent unwinding angles (ϕ_{ap}) for simultaneously decreasing conjugate and plasmid concentrations (Figure 2.7c). The actual unwinding angles (ϕ), determined from the ordinate intercepts in Figure 2.7c, are 14.5^{o} and 15.3 ^{o} for conjugates **1** and **4**, respectively. Polyamide controls **5a** and **5b**, which lack an acridine intercalator, showed no unwinding of pUC19.

The unwinding assay provides evidence that the conjugates are simultaneously intercalated and bound to the minor groove. Since parent hairpin polyamides had no effect on DNA unwinding, the total unwinding is attributed to the tethered intercalating moiety. The helical unwinding angle (ϕ) of the polyamide-DACA conjugate **4** was consistent with reported values for the unconjugated intercalator, indicating that conjugation using the trioxa-diamine linker (To) does not compromise the propensity of intercalation. However, conjugate **1** showed an average ϕ of ~2.5^{o} less than the reported

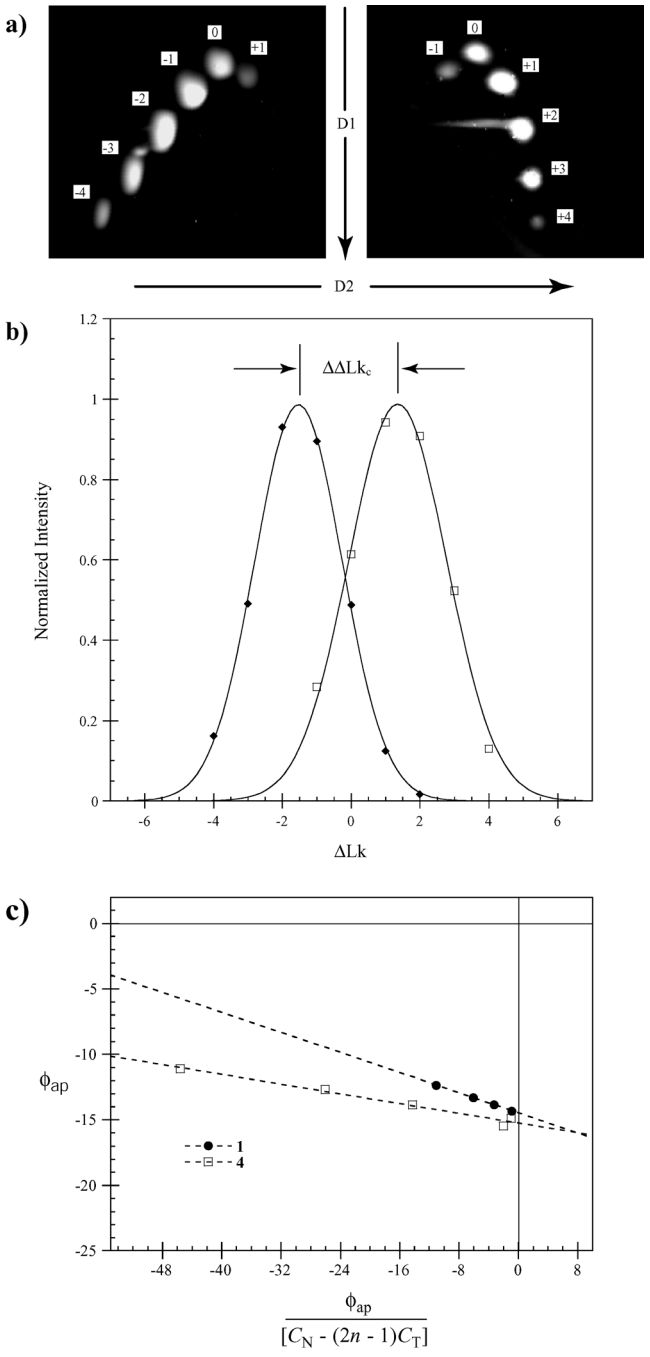

Figure 2.7 (a) Images of topoisomer bands from reactions containing and lacking polyamide-acridine conjugate **1**, (top left and top right, respectively). The directions of electrophoresis and ΔLk values are shown. (b) The corresponding Boltzman distributions (extracted from normalized band intensities) are shown below their gels. (c) Binding isotherms for polyamide-acridine conjugates **1** (•) and **4** (□). Each data point was calculated from one set of distributions (as in part a). The ordinate intercept yields the canonical unwinding angle (ϕ) per polyamide-acridine conjugate.

value for 9-aminoacridine.[37] The attenuated ϕ of conjugate **1** suggests that the slightly shorter linker (Do) may not be optimal for maximum occupancy of the intercalator moiety within DNA –in agreement with the DNase I footprinting data. The polyamide may disrupt the orientation of the intercalator within the base-pair stack resulting in the slight decrease in ϕ. We cannot rule out that the difference in unwinding properties of the acridine intercalator may be explained by the changes in chromophore electronics such as the enhanced electrostatic associations upon conjugation.

Effects of Polyamide-Acridine Conjugates on Major-Groove Protein-DNA Complex Formation

The ability of polyamide-acridine conjugates to selectively inhibit the association of a major-groove binding protein with DNA was tested using the basic DNA binding domain of the GCN4 (222-281) homodimer.[47] Inhibition was first determined by performing an EMSA of the ^{32}P radiolabeled 33-bp DNA duplex, ARE-41, which contains a GCN4-binding site (5'-CTGACTAAT-3')[17] and a single flanking polyamide binding site (5'-TGGGTA-3') oriented such that the acridine moieties of the bound polyamides **1-4** were directed toward the TF binding site. All four polyamide conjugates significantly inhibited GCN4-DNA complex formation. Representative gels show shifted bands from complexed to free DNA for compounds **1-3** as the conjugate concentrations were increased from 1nM to 1μM in the presence of 200 nM concentration of GCN4 (Figure 2.8a, lanes 3-15). The mobility of the DNA duplex was unaffected by the addition of polyamide alone (Figure 2.8a, lane 16). Quantitation of shifted lanes by comparison to control lane 2 (containing only DNA and GCN4) provides percent inhibition curves (Figure 2.8b). Conjugates **1** and **3** were the most effective of the series

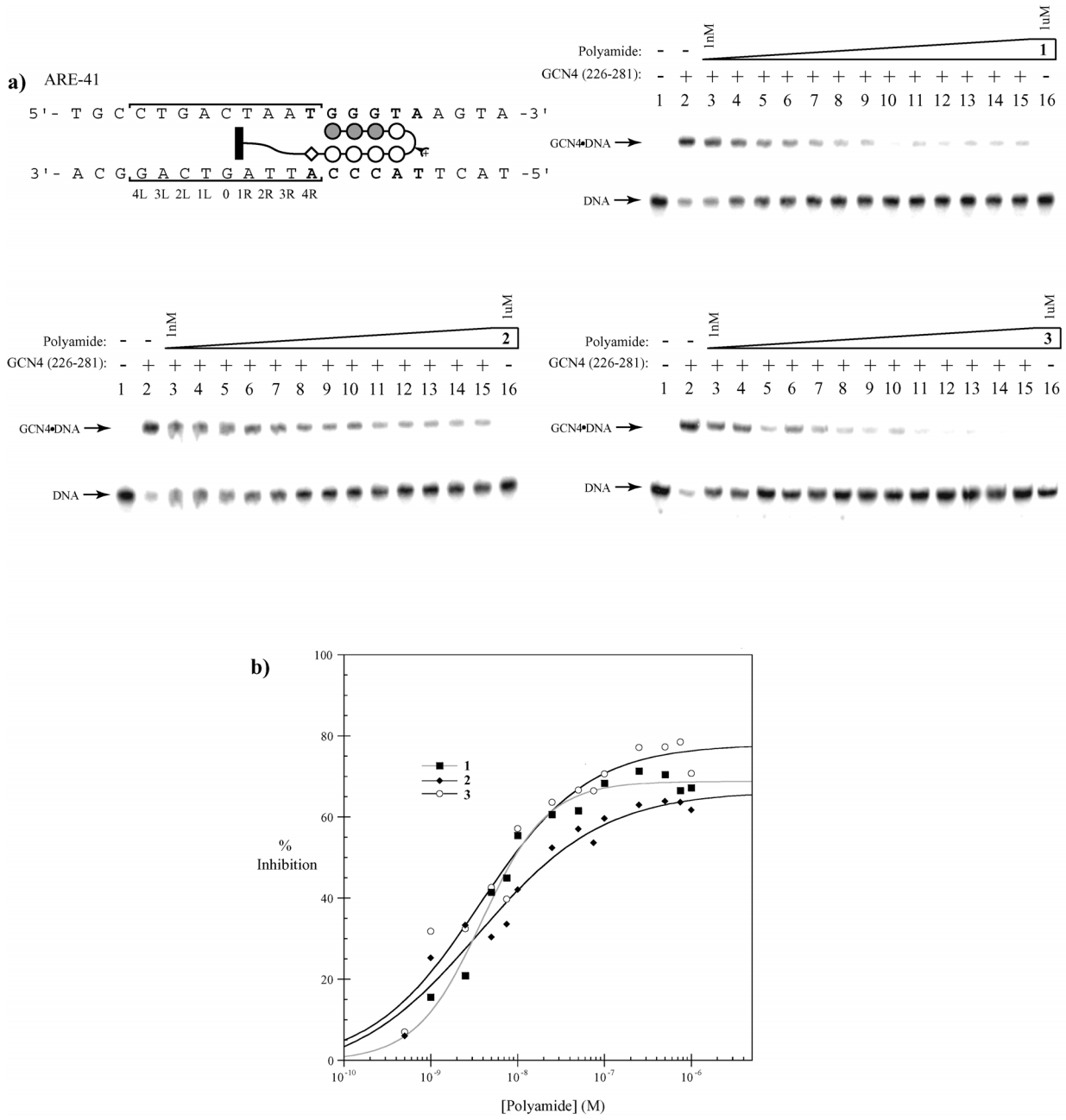

Figure 2.8 (a) Representative GCN4 (222-281) electrophoretic mobility shift assay results for conjugates **1**, **2**, and **3** with ARE-41. The pseudopalindromic GCN4 binding site is shown in brackets and the base pair assignments are shown below the duplex. The polyamide binding site is shown as bold text. Polyamide symbols are as in Figure 2.2. The storage phosphor autoradiograms of **1-3** are shown below the duplex with visibly shifted bands in the presence of increasing concenterations of polyamide-conjugate. Upper band, GCN4 (222-281)-DNA complex; lower band, free DNA; lane 1, DNA only; lane 2, DNA incubated with 100 nM GCN4 (222-281); lanes 3, 4, 5, 6, 7, 8, 9, 10, 11, 12, 13, 14, and 15 are 100 nM GCN4 (222-281) and 1 nM, 2.5 nM, 5 nM, 7.5 nM, 10 nM, 25 nM, 50 nM, 75 nM, 100 nM, 250 nM, 500 nM, 750 nM, and 1 μM **1**, **2**, or **3**, respectively; lane 16, DNA with 1 μM polyamide. (b) Inhibition curves for polyamide conjugate effects on formation of GCN4 (222-281)-DNA complex.

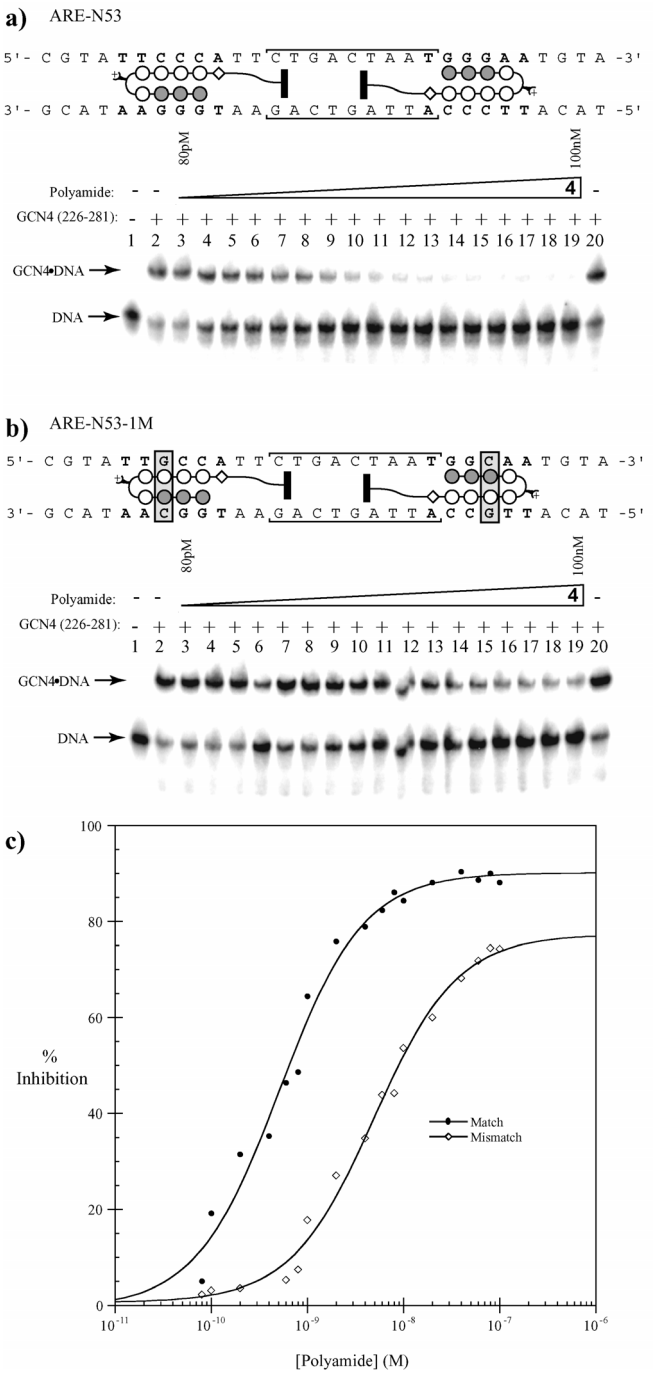

Figure 2.9 Representative GCN4 (222-281) electrophoretic mobility shift assay results for conjugate **4** with (a) duplex ARE-N53 containing two polyamide match sites and (b) duplex ARE-N53-1M containing two single base-pair mismatch sites. Symbols for polyamides are indicated in Figure 2.2. Lane 1, DNA only; lanes 2 and 20, DNA incubated with 100 nM GCN4 (222-281); lanes 3, 4, 5, 6, 7, 8, 9, 10, 11, 12, 13, 14, 15, 16, 17, 18, and 19 are 100 nM GCN4 (222-281) and 80 pM, 100 pM, 200 pM, 400 pM, 600 pM, 800 pM, 1 nM, 2 nM, 4 nM, 6 nM, 8 nM, 10 nM, 20 nM, 40 nM, 60 nM, 80 nM, and 100 nM **4**. (c) Inhibition curves for polyamide-conjugate effects on formation of GCN4 (222-281)-DNA complex with two flanking polyamide match sites (solid circles) and two flanking polyamide mismatch sites (open diamonds).

(65-80% complex inhibition) with IC_{50} values of ~10 nM. Conjugate **2** showed 60-65% inhibition while compound **4** attained slightly less than 60% complex inhibition. Control compounds **5a** and **5b** corresponding to polyamides containing PEG diamine linkers, but lacking acridine or DACA, were unable to inhibit GCN4 binding.

Inhibition studies were then carried out using the 40-bp duplex ARE-53. This duplex contains the same GCN4 and polyamide binding site as ARE-41, with an additional flanking polyamide binding site proximal to the GCN4 binding domain (Figure 2.9a). The effects of two binding conjugates increased the TF inhibition of all compounds to near quantitative amounts[48] while reducing the IC_{50} values to sub-nanomolar concentrations. Conjugates tested on the analogous ARE-53-1M duplex (Figure 2.9b), containing internal single base-pair mismatches (as with sites **II** and **IV** on pEF10) at both polyamide binding sites, resulted in more than 20% decreased inhibition and increased IC_{50} values (>10 nM, Figure 2.9c).

Gel mobility shift experiments on conjugates **1-4** show that **1** and **3** effectively inhibit major-groove binding of GCN4. CPK modeling suggests that the intercalation site with these compounds extends between three and four base pairs past the β-alanine unit of the polyamide. On the basis of published GCN4 basic region-DNA crystal structures,[10,11] it is an interesting exercise to speculate on the local topological perturbations caused by site-specific intercalation (Figure 2.10). Between base-pair sites 0 and 1R the conjugate may locally disrupt two phosphate interactions (Arg243 and Thr236), one hydrophobic interaction (Ala239), and one hydrogen bond (Arg243) of right-half site GCN4 monomer. Additionally, a phosphate interaction (Arg240) and hydrogen bond (Arg243) at the center of binding (position 0) from the left-half site

monomer may be altered. This arginine contact is considered crucial for anchoring the protein to the center of the binding site. Besides the immediate contacts affected, more distal allosteric disruptions, such as widening of the major groove and increased relative twist of the two ends of the duplex by intercalation, may contribute to the decreased affinity of GCN4. The slightly lower GCN4 inhibition by conjugates containing longer linkers **2** and **4** may be accounted for by intercalation at other sites and failing to unwind the duplex at the specified contacts.

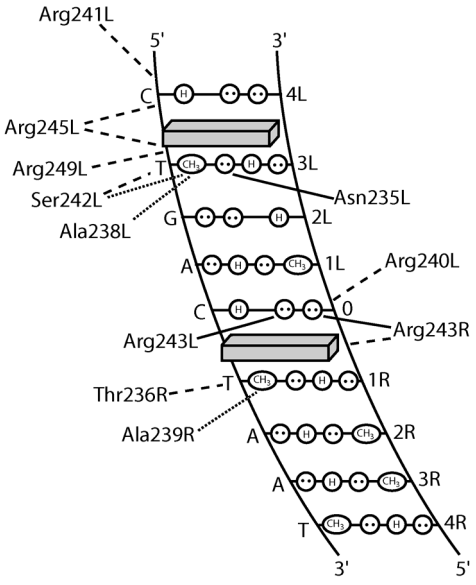

Figure 2.10 Predicted major-groove contacts of the GCN4 dimer directly affected by intercalation of **3** or **4** in ARE-N53. Intercalating chromophores are shown as shaded blocks. Protein side-chain contacts made by the left-half site monomer end with L while contacts made by the right-half site monomer end with R. The CG base pair at position 0 represents the center of the DNA pseudodyad. Solid lines represent hydrogen bonds, dashed lines represent phosphate contacts, and dotted lines represent van der Waals interactions. Circles with two dots depict the lone pairs of the N7 of purines, the O4 of thymine, and the O6 of guanine. Circles containing an H represent the N6 and N4 hydrogens of the exocyclic amines of adenine and cytosine, respectively. The C5 methyl group of thymine is shown as a circle with CH_3 inside.

The duplex ARE-53, containing a second polyamide binding site, provided increased inhibition of GCN4. The proposed intercalation site for the added conjugate with dioxa-diamine linkers **1** or **3** falls between the 3L and 4L base pairs. This site houses a large concentration of critical contacts, including four phosphate interactions (Arg241, Arg245, Arg249, and Ser242), two hydrophobic interactions (Ser242 and Ala238), and one hydrogen bond (Asn235), lying deep within the major groove. Overall, the combined effect of both intercalation sites could be the direct

disruption of nearly one-half of the identified contacts of the GCN4 complex. The longer linked trioxa-diamine conjugates **2** and **4** showed equal inhibition, indicating that the precise location of critical GCN4 contacts relative to intercalation is not as crucial when two conjugate binding sites are present. The duplex containing one core mismatch for each binding site (ARE-53-1M) demonstrates inhibition selectivity with an IC_{50} value of approximately one order of magnitude higher than its corresponding match sequence in agreement with mismatch affinities from DNase I footprinting results.

Effects of Polyamide-Acridine Conjugates on Sp1/Sp3•DNA Complex Formation

To demonstrate the versatility of polyamide-intercalator conjugate inhibition of transcription factor complex formation, an additional EMSA study using cellular extract containing the zinc finger Sp1/Sp3[49] was investigated. The synthetic radiolabeled 32bp DNA duplex, SP1R, containing the Sp1/Sp3 consensus "GC Box" binding site (5'-GGGGCGGGGC-3') and a single flanking polyamide binding site spaced identical in fashion to ARE-41 was treated with **1** prior to equilibration with HeLa nuclear extract. Visibly shifted bands are evident in Figure 2.11, indicating complexed and free probe. As polyamide concentration is increased from 100pM to 1uM, the percent complex intensity is reduced to virtually zero. A control lane containing **5c** shows no inhibition relative to the bands containing extract without polyamide.

The gel mobility shift experiments of Sp1/Sp3•DNA complexes provide an additional example of transcription factor inhibition by polyamide-intercalator conjugates. The Sp1/Sp3 consensus binding sequence strictly consists of guanine and cytocine base pairs which have been traditionally challenging sequences to target in the

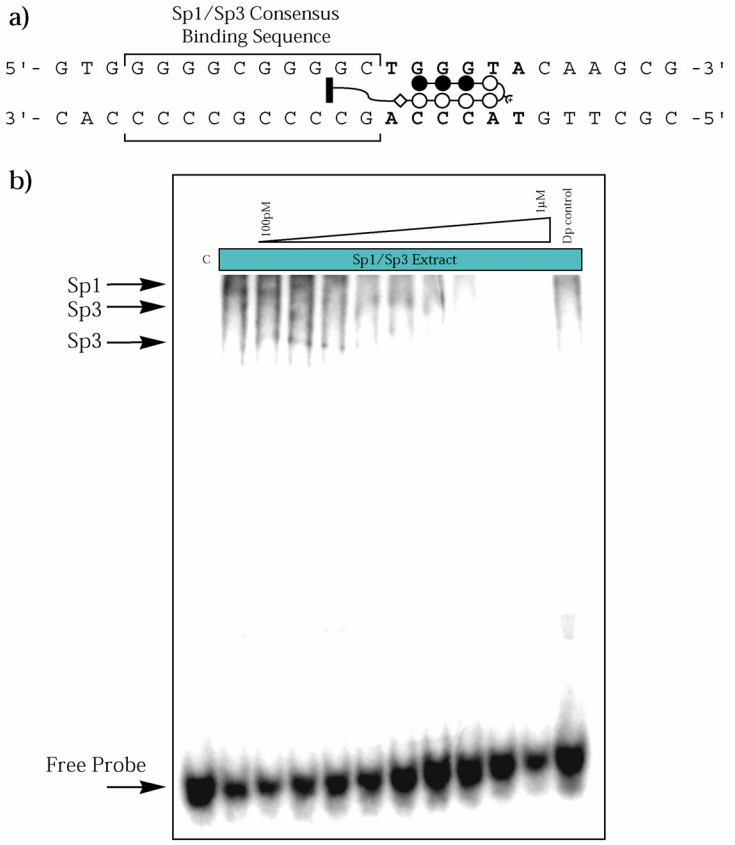

Figure 2.11 Sp1/Sp3 electophoretic mobility shift assay for conjugate **1** with SP1R. a) The Sp1/Sp3 concensus binding site is shown in brackets while the polyamide binding site is shown as bold text. b) Upper band, Sp1/Sp3•DNA complex; lower band, free DNA (probe); lane 1, DNA only; lane 2, DNA incubated with HeLa nuclear extract; lanes 3-11 are HeLa nuclear extract with DNA and 100, 500 pM, 1, 5, 10, 50, 100, 500 nM and 1 μM **1**. lane 12, HeLa nuclear extract with DNA and 1 μM **1**.

field of polyamide recognition. Using polyamide-intercalator conjugates to bind an easily recognized sequence flanking the consensus site and deliver a tethered intercalator moiety provides an attractive approach to disrupt the Sp1/Sp3•DNA complex.

Topoisomerase II Inhibition Studies

The ability of polyamide-intercalator conjugates to selectively trap the topoisomerase II enzyme[50] and subsequently cause transient double strand breaks at the polyamide binding sites was explored using the *Topo*Gen, Inc. topoisomerase II drug screening kit. The assay utilizes human topoisomerase IIα p170 to observe the effects on

closed-circular pRYG with drug candidates. Briefly, conjugates **1**, **3**, and controls (known topoisomerase II inhibitors: etoposide and m-AMSA) were separately equilibrated with supercoiled pRYG prior to addition of the topoisomerase II enzyme. After relaxation the enzymatic reactions were halted with the addition of SDS followed by treatment with proteinase K to digest any covalently attached enzyme from the nicked DNA. Enzyme and intercalator conjugate were removed by chloroform extraction and

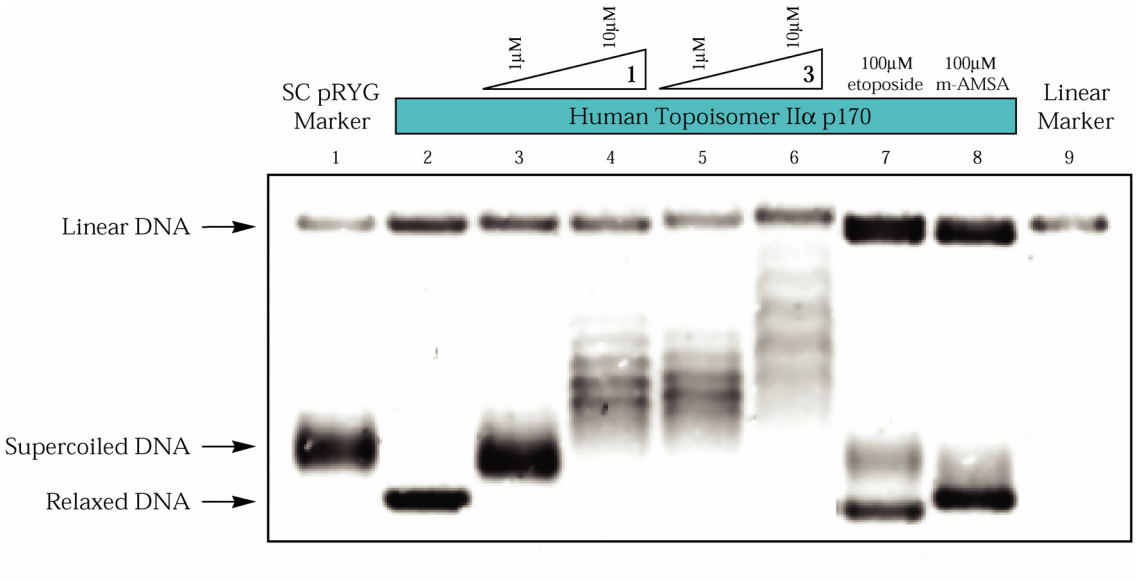

Figure 2.12 Topoisomerase II assay results for conjugates **1** and **2** on supercoiled pRYG plasmid. Lane 1, supercoiled pRYG marker; lane 2, pRYG treated with topoisomerases II; lanes 3-6, pRYG treated with topoisomerase II and polyamide conjugates; lanes 7-8, pRYG treated with topoisomerase II and contol inhibitors; lane 9, linear pRYG. Under EtBr conditions, relaxed DNA is expected to migrate faster than supercoiled DNA

run on a 1% agarose gel containing ethidium bromide. As shown in Figure 2.12, treatment of topoisomerase II with conjugates 1 and 2 showed blurred bands of supercoiled DNA and no increase in linear DNA formation relative to form I DNA. As expected, topoisomerase II controls showed substantial increases in linear DNA formation.

These inhibition studies show that the polyamide-intercalator conjugates tested do not significantly trap the human topoisomerase IIα p170 dimer in the covalent stage of the transient DNA breaking process.[50] Although the exact mechanisms of known topoisomerase II poisons are unknown, is has been postulated that the substituents projecting out of the minor groove from chromophore intercalation are partially responsible.[50] Studies have shown that substituent isomers (i.e., o-AMSA vs. m-AMSA) vary greatly in their propensity of topoisomerase II inhibition.[51] It's not unlikely that the attachment of a large polyamide at this position would show lack of inhibition. The gel in Figure 2.12 does show topoisomerase bands, presumably differing in linking number by +/- 2, which provides more evidence to support the intercalation model for conjugates **1** and **2**.

Alternative Polyamide-Acridine Motif

The inherent asymmetry of the hairpin polyamide binding motif and the energetic penalty when the "turn" monomer is placed over a G•C base-pair limits the number of sequences that a polyamide-intercalator conjugate can target when tethered off the C-terminus. To broaden the scope of possible sequences targeted with specific intercalators, a new motif was synthesized where the PEG linker and acridine are linked off the DABA turn (Figure 2.13). Starting from ImImImPy-(*R*)^{NHFmoc}*γ*-PyPyPyPy-*β*-Pam-resin, the Fmoc-protected DABA "turn" monomer was deprotected by treatment with piperidine and coupled to activated Fmoc-8-Amino-3,6-Dioxaoctonoic Acid. This resin-bound polyamide was then subjected to aminolytic cleavage using the *N,N*'-(dimethylamino)propylamine to form **7**. After reverse-phase HPLC purification, the polyamide primary amine was allowed to react with 9-chloroacridine in phenol at

elevated temperature in the presence of diisopropylethylamine (DIEA) and the desired conjugate **8** was purified by preparatory reverse-phase HPLC.

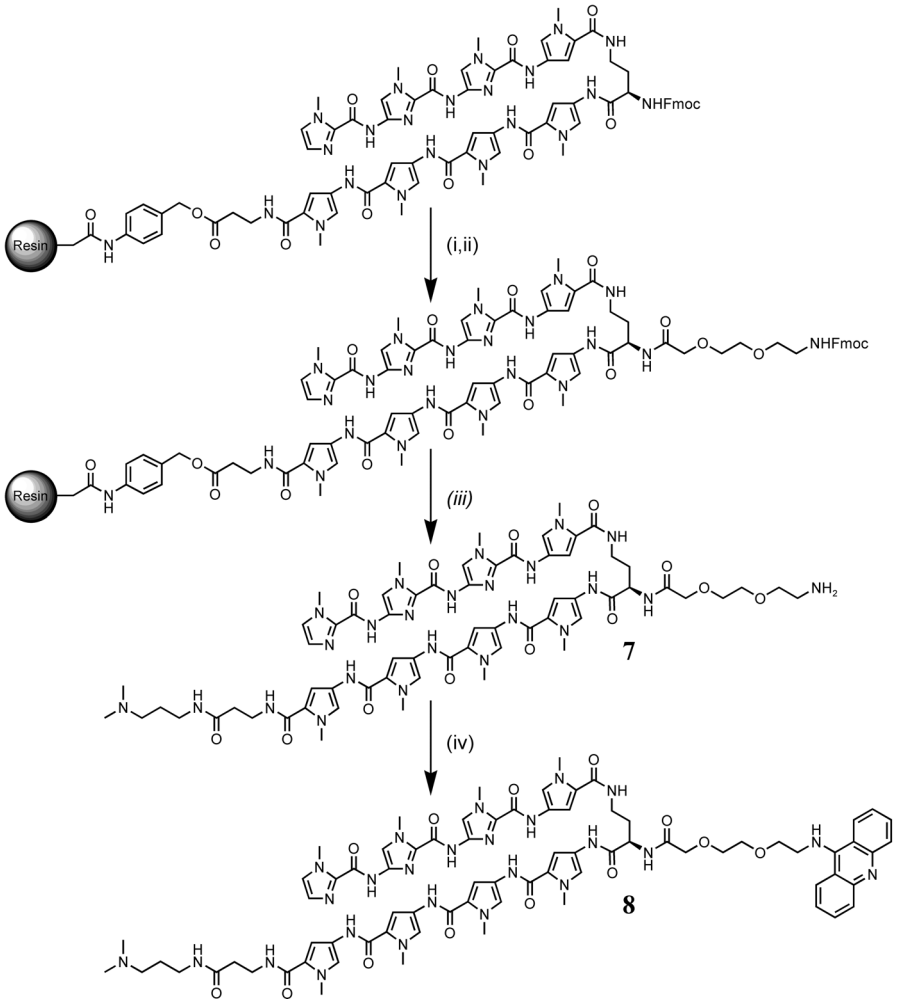

Figure 2.13 Synthetic scheme for polyamide-acridine turn-linked conjugates: (i) 4:1 piperidine-DMF, 25°C (30 min); (ii) Fmoc-8-Amino-3,6-Dioxaoctonoic Acid, HBTU, DIEA, NMP, rt (30 min); (iii) *N,N'*-(dimethylamino)propylamine, 55°C (18 h); (iv) 9-chloroacridine, phenol, DIEA, 100°C (1 h).

Quantitative DNase I footprint titrations were again performed on a 5'-^{32}P-labeled PCR-amplified fragment of pEF10 (Figure 2.5) to determine the equilibrium association constants (K_a). DNase I footprinting results show that both **7** and **8** are capable of binding their designed sites with high affinity and specificity (Figure 2.14). The affinity of the acridine conjugate **8** was found to be ~3-fold higher than the unconjugated **7** (K_a =

2.0×10^{10} M^{-1} for **8** and $K_a = 7.0 \times 10^9$ M^{-1} for **7**), suggesting that the intercalator moiety contributes to binding, likely from intercalation. Both compounds display greater than 10-fold specificity over single base-pair mismatch sites.

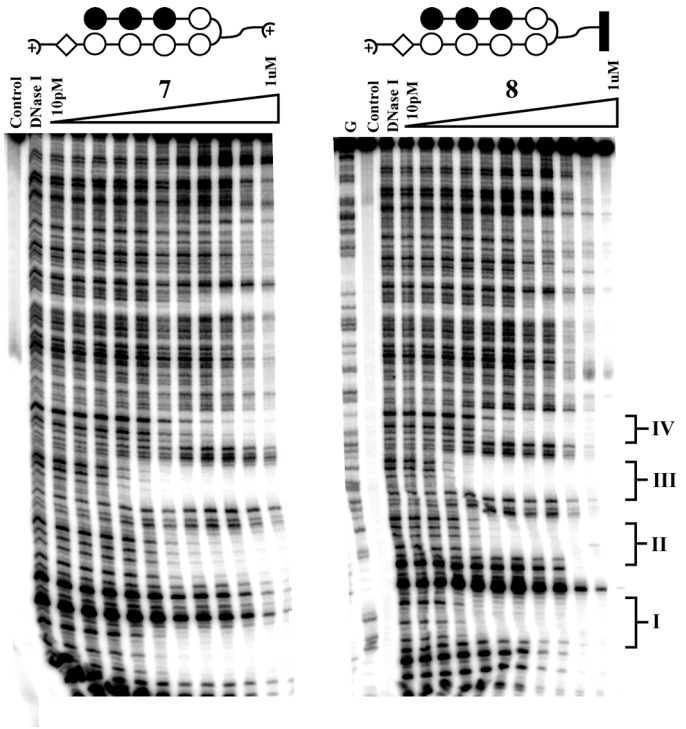

Figure 2.14 Quantitative DNase I footprint titration experiments with **7** and polyamide-acridine conjugate **8** on the PCR-amplified 5'-^{32}P-labeled 276-bp fragment of pEF10. **I**, **II**, **III**, and **IV** correspond to the sites indicated in Figure 2.5.

In vitro Transcription Inhibition

Polyamide-intercalator conjugates were then tested for their ability to inhibit the prokaryotic T3 RNA polymerase (Figure 2.15).[52] The T3 polymerase recognizes the sequence 5'-AATTAACCCTCACTAAAGGG-3' which contains the polyamide binding site 5'-WGGGWW-3'. A system was constructed using $_p$bc KS+ where the T3 polymerase elongates one strand toward a T7 promoter site, while the T7 promoter (added as an internal control) elongates the complementary strand in the opposite

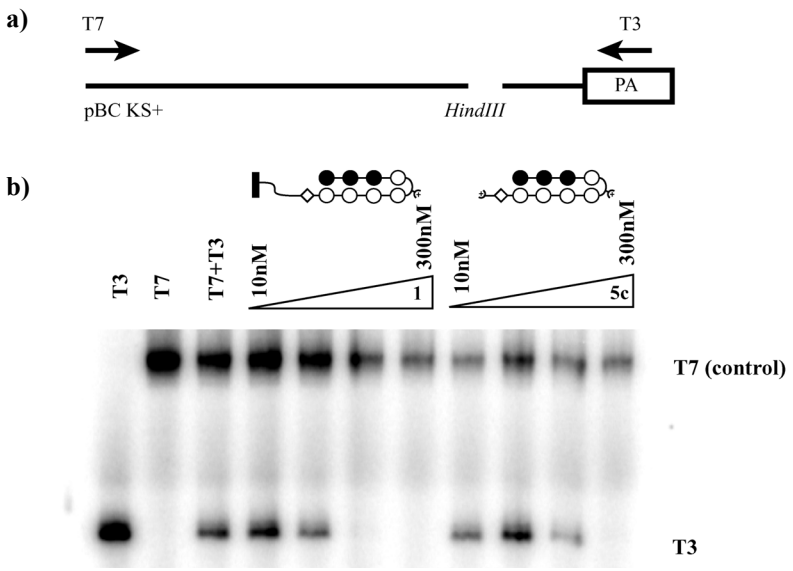

Figure 2.15 Transcription run-off experiments for conjugates **1** and **5c** on a *Hind* III restricted pBC KS+ plasmid. a) Schematic of the plasmid sequence showing polymerase and polyamide binding sites. b) Transcript run-offs for T7 (longer sequence) and T3 (shorter sequence) in the presence and absence of polyamide.

direction toward the T3 promoter site. Prior to elongation, the plasmid was restricted with *Hind* III at an off-center site between the two promoters to allow runoff experiments with different length mRNA (incorporated with [α-^{32}P]-rUTP). Gel electrophoresis (Figure 2.15) shows that plasmid equilibrated with unconjugated polyamide **5c** inhibits T3 elongation at ~300nM while plasmid equilibrated with the polyamide-acridine conjugate **1** inhibits elongation at only 100nM. In both cases, elongation of the control T7 polymerase is unaffected.

Cellular Uptake Properties of Fluorescein-Linked Polyamide-Acridine Conjugates

The effectiveness of polyamide-intercalator conjugates as useful tools in molecular biology and in a cellular context requires that they be permeable to the outer membrane and gain access to the nucleus of living cells.[53,54] To study the cellular uptake properties of this new class of compounds, a series of polyamide-acridine conjugates

incorporating the fluorophore Bodipy FL or fluorescein was synthesized (Figure 2.16). The intracellular distribution of these molecules in several cell lines was then determined by confocal laser scanning microscopy.

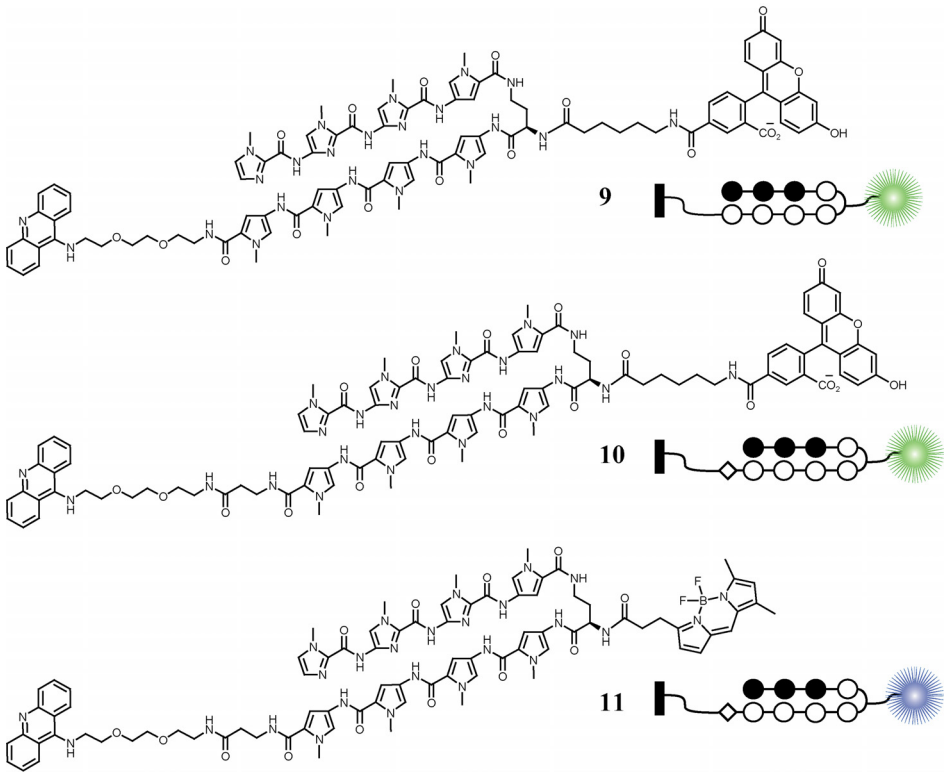

Figure 2.16 Structures of acridine conjugates used in cellular uptake experiments.

The fluorescent conjugates **9** and **10**, containing carboxyfluorescein (FAM), were able to penetrate the nuclear membrane of several cell lines (Table 2.3). Compound **10** appears to localize readily in LN-CaP and MEG-01 cell lines while compound **9** was confined to the media. Interestingly, these results suggest that the additional β-alanine residue does not hinder cellular uptake when coupled to a compound containing acridine, contrary to the results found with polyamides lacking acridine.[53,54] The Bodipy containing conjugate **11** showed exclusion from the nucleus of all tested cell lines except the S194 mouse myeloma B-cell line (Figure 2.17). These combined results suggest that

the acridine conjugates may be useful for cellular studies if linked to the proper fluorophore for a given cell line.

Table 2.3 Cellular localization data for polyamide-acridine conjugates in tested cell lines*.

polyamide	MCF-7	HeLa	PCL3	LN-CaP	SK-BR-3	DLD-1	786-O	293	Jurkat	CEM	MEG-01	MEL	NB4	3T3
9	+	+	+	--	+	+	+	+	+	+	--	--	--	N/A
10	++	++	++	+	+	+	+	+	++	++	++	--	--	N/A

* + +, Nuclear staining exceeds that of the medium; +, nuclear staining less than or equal to that of the medium but still prominent; -, very little nuclear staining with the most fluorescence seen in the cytoplasm and/or medium; --, no nuclear staining.

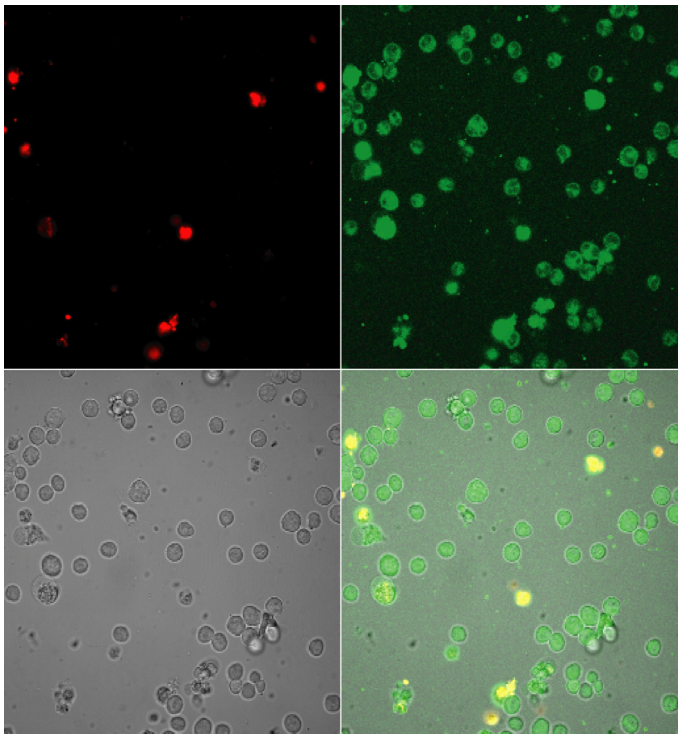

Figure 2.17 . Cellular localization of polyamide-acridine bodipy conjugate **11** in S194 cell line. *Top left*: dead cell stain Sytox Orange (0.5μM). *Top right*: conjugate **11** (5 μM), Hoechst dye 33342 (50 μM). *Bottom left*: visible light image (greyscale). *Bottom right*: overlay.

Cellular Uptake Properties of Polyamide-Acridine Orange Conjugates

One shortcoming of using fluorophore-linked polyamides to infer uptake properties of parent compounds is that the addition of the fluorophore itself will likely change the propensity for uptake into the cell. Additionally, attachment of fluorescein to

polyamides has shown marked decreases in affinity relative to the parent (usually > 10-fold). Intrinsically fluorescent polyamides would provide a useful means of monitoring the *actual* compound desired for cellular studies. However, to date no viable polyamides have been synthesized that produce a sufficient signal upon excitation for detection within the cell. Polyamide-intercalator conjugates offer an additional platform for fluorescence studies by way of the acridine chromophore.

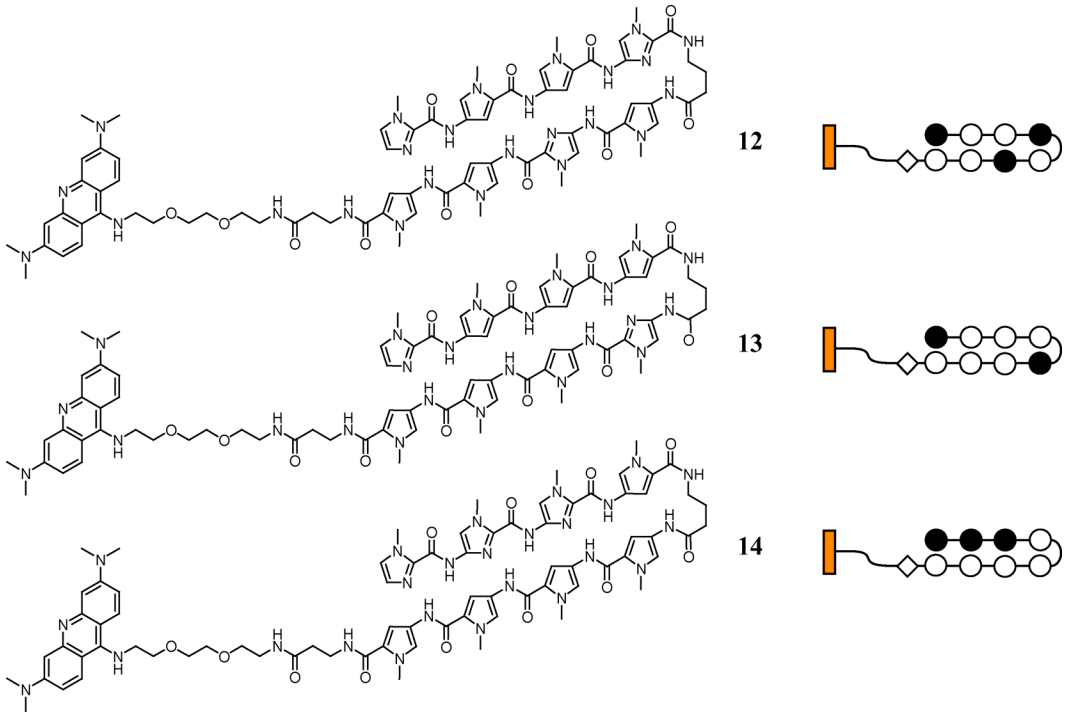

Figure 2.18 Structures of polyamide-acridine orange conjugates used in cellular uptake experiments.

Acridine orange has a similar structure to the acridine intercalator (two additional exocyclic amino groups at the 3 and 6 positions) yet with substantially superior fluorescence emission properties.[55] This cell-permeant nucleic acid binding dye is known to emit green fluorescence when bound to dsDNA and red fluorescence when bound to ssDNA or RNA.[55] The substitution of acridine orange for acridine in polyamide-intercalator conjugates would likely afford a means to detect specific binding

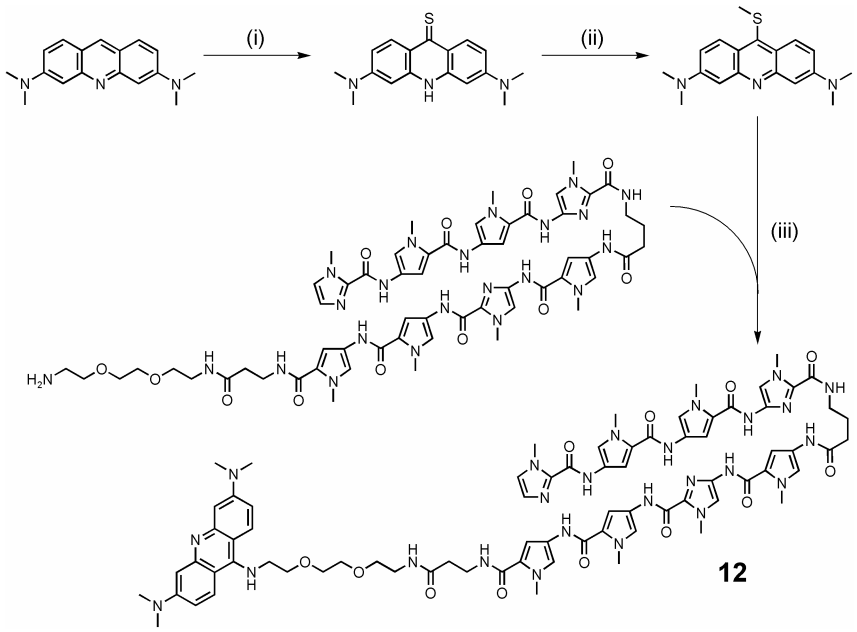

Figure 2.19 Synthetic scheme for polyamide-acridine orange conjugates: (i) Sulfur, 220°C (30 min); (ii) $NaOCH_2$, MeI, 50°C (30 min); (iii) phenol, DIEA, 100°C (30 min).

Table 2.4. Cellular localization data for polyamide-acridine orange conjugates in tested cell lines*.

polyamide	MCF-7	HeLa	PCL3	LN-CaP	SK-BR-3	DLD-1	786-O	293	Jurkat	CEM	MEG-01	MEL	NB4	3T3
12	-	+	+	N/A	N/A	N/A	-	-	+	+	+	+	+	+
13	+	+	+	N/A	N/A	N/A	+	--	+	+	+	+	+	+
14	--	-	+	N/A	N/A	N/A	--	-	+	+	+	+	+	-

* + +, Nuclear staining exceeds that of the medium; +, nuclear staining less than or equal to that of the medium but still prominent; -, very little nuclear staining with the most fluorescence seen in the cytoplasm and/or medium; --, no nuclear staining.

intercalators within the cell. To this end a series of polyamide-acridine orange conjugates differing in imidazole content and location were synthesized (Figures 2.18 and 2.19). The absorbance and emission spectra (Figure 2.20) show the favorable fluorescence properties for cellular uptake studies.

The series was equilibrated and screened with a small panel of cell lines to assay for nuclear uptake. All three compounds localized in the nucleus of Jurkat, CEM, MEG-01, MEL, NB4, 3T3, HeLa, and PC3 cells (Table 2.4). A representative image of cellular uptake for compound **13** in PC3 cells is shown in Figure 2.21. Additionally, compound

13 was nuclear in MCF-7 and 786-0, signifying that the arrangement of imidazole rings is significant for uptake with this series. The ability of the acridine orange conjugates to localize in the nucleus of various cell lines suggests that this architecture may be useful for *in vivo* studies.

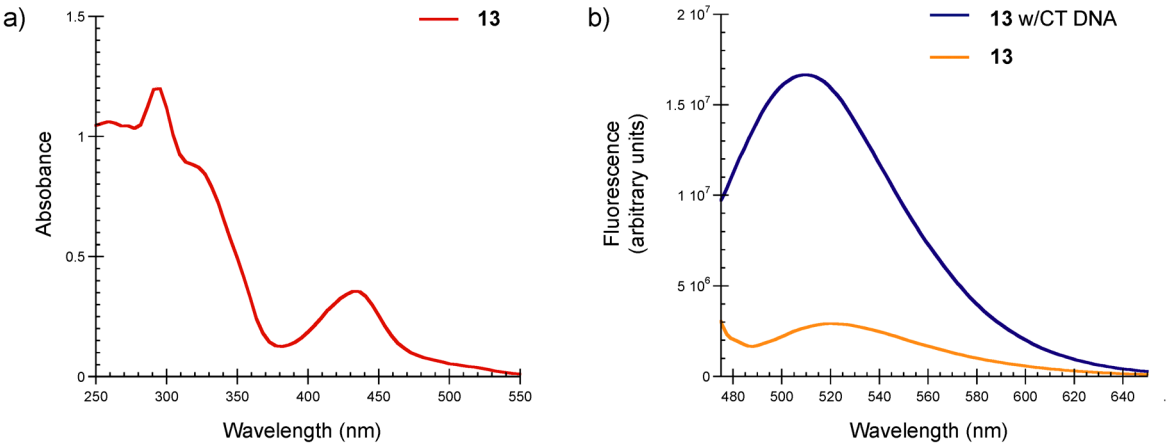

Figure 2.20 (a) Absorption spectra of free polyamide-acridine orange conjugate **13**. (b) Fluorescence emission profile for polyamide-acridine orange conjugate **13** in the prescence and absence of CT DNA.

Discussion

There are several examples of DNA-binding natural products, such as actinomycin D and triostin A, which use bimodal cooperative intercalation/groove binding for molecular recognition of DNA.[56-58] Early design efforts toward artificial mimics of these natural products combined modules of intercalators (such as acridine or phenoxazone) and groove binders derived from netropsin and distamycin.[59-61] Intercalators and minor-groove binding polyamides affect DNA conformation in very different ways. Intercalators unwind and extend the helix by 3.4 Å while crescent-shaped minor-groove binders disrupt the DNA minimally, maintaining a relatively undistorted shape of the B-form helix.[28,29] DNA structural distortion remote from the site of intercalation and extending over four base pairs could possibly disrupt essential minor-

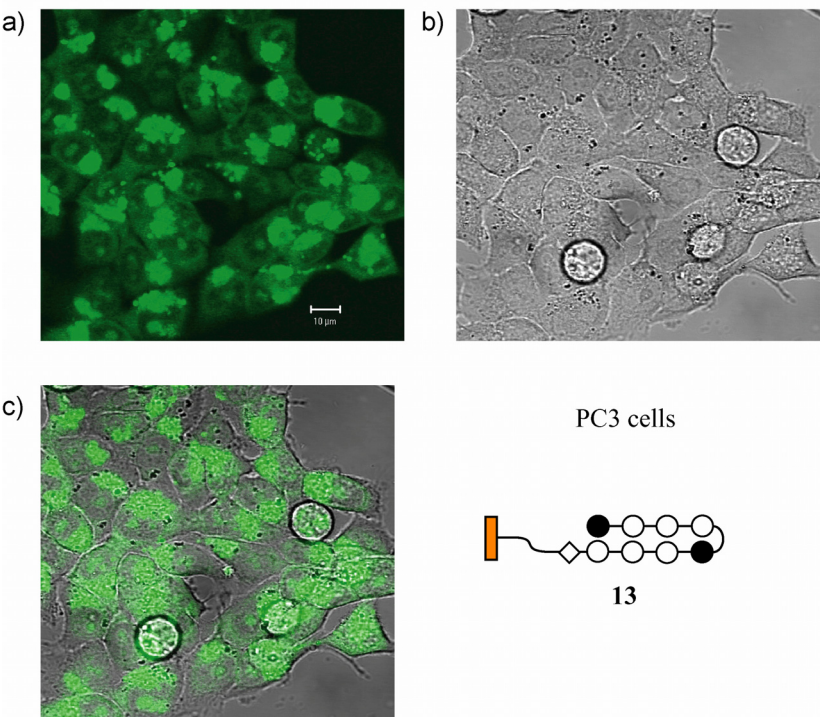

Figure 2.21 Cellular localization of polyamide-acridine orange conjugate **13** (5μM, 10-14h) in PC3 cell line. a) polyamide-acridine orange **13**, b) visible light image (greyscale) and c) overlay.

groove contacts by the polyamide ring pairs. Therefore, the choice of linker length and flexibility is crucial for optimum cooperative binding of both modules. Indeed, one would prefer that the two binding domains function independently, i.e., the polyamide defines the target sequence with little sequence preference superimposed by the intercalator, and the intercalator unwinds locally with little constraint from the adjacent polyamide.

Here we show that hairpin polyamide-acridine conjugates are capable of selectively inhibiting a protein binding exclusively to the major groove. The conjugates intercalate and bind to the minor groove without sacrificing affinity or specificity. By delivering an intercalating moiety to a specified region of DNA from a tethered polyamide, this class of molecules should be a general method for targeting a broad array of protein-DNA complexes of interest. Initial *in vitro* transcription and cellular uptake

results show that these compounds may be potentially useful in regulating gene expression of living cells.

Experimental Section

Materials

9-Chloroacridine was purchased from Pfaltz & Bauer, Inc. *N*-(2-(Dimethylamino)ethyl)-9-chloroacridine-4-carboxamide was synthesized according to published procedures.[41] Restriction endonucleases were purchased from New England Biolabs and used as noted in the manufacturer's protocol. Sequenase (version 2.0) was obtained from Boeringher-Mannheim. [α-^{32}P]-Thymidine-5'-triphosphate (≥3000 Ci/mmol) and [α-^{32}P]-deoxyadenosine-5'-triphosphate (≥6000 Ci/mmol) were purchased from DuPont/NEN. [γ-^{32}P]-Adenosine-5'-triphosphate (≥6000 Ci/mmol) was obtained from ICN. Purified pUC19 DNA for unwinding angle determination was isolated from transformed JM109 *Escherichia coli* using the Qiagen protocol. EDTA, dithiothreitol (DTT), ultrapure agarose, and calf thymus topoisomerase I and topoisomerase II were purchased from GIBCO/BRL. T3 and T7 polymerase were purchased from Promega. Micron 50 microconcentrators were purchased from Amicon. ProbeQuant G-50 micro columns were purchased from Amersham Pharmacia Biotech, Inc. GCN4 (222-281) prepared by solid-phase synthesis was generously provided by Martha G. Oakley. Water (18 MΩ) was obtained from a Millipore MilliQ water purification system, and all buffers were 0.2 μm filtered. Reagent-grade chemicals were used as received unless otherwise stated.

UV spectra were measured on a Beckman-Coulter DU7400 diode array spectrophotometer. Matrix-assisted, laser desorption/ionization time-of-flight mass

spectrometry (MALDI-TOF) was performed using an Applied Biosystems Voyager DE-Pro. HPLC analysis was performed on a Beckman Gold system using a RAININ C_{18}, Microsorb MV, 5 μm, 300 × 4.6 mm reversed-phase column in 0.1% (v/v) TFA with acetonitrile as eluent and a flow rate of 1.0 mL/min. Preparatory reversed-phase HPLC was performed on a Beckman HPLC using a Waters DeltaPak 25 × 100 mm, 100 μm C_{18} column equipped with a guard, 0.1% (wt/v) TFA, 0.25% acetonitrile/min.

ImImImPy-(R)$^{H2N}\gamma$-PyPyPyPy-β-Do-Acr (1)

Compound **6a** (1 μmol aliquot) was added to 100 μL of phenol and dissolved by heating to 100°C. To this solution was added 9-chloroacridine (0.5 M, 3 μL) in DMF, followed by 10 μL of DIEA, and the reaction was allowed to proceed at 100°C for 1 h. The mixture was then cooled to 50°C and diluted with 0.1% (wt/v) TFA (100 μL). The mixture was then further cooled to room temperature and treated with 1 mL of 80% TFA/DCM, 0.4 M PhSH. After 30 min the mixture was diluted with 0.1% (wt/v) TFA and the resulting solution purified by reversed-phase HPLC. Lyophilization provided ImImImPy-(*R*)$^{H2N}\gamma$-PyPyPyPy-β-Do-Acr (**1**) as a yellow powder (0.50 mg, 41% recovery). MALDI-TOF-MS (monoisotopic) calcd for $C_{71}H_{81}N_{24}O_{12}$ (M+H): 1461.7. Found: 1461.7.

ImImImPy-(R)$^{H2N}\gamma$--PyPyPyPy-β-To-Acr (2)

Synthesized as described for **1** starting from 1 μmol of **6b** (0.41 mg, 35% recovery). MALDI-TOF-MS (monoisotopic) calcd for $C_{71}H_{81}N_{24}O_{12}$ (M+H): 1533.7. Found: 1533.7.

ImImImPy-(R)^{H2N}γ-PyPyPyPy-β-Do-DACA (3)

Synthesized as described for **1** using *N*-(2-(dimethylamino)ethyl)-9-chloroacridine-4-carboxamide (0.5 M, 3 μL) followed by the addition of 20 μL of DIEA (0.37 mg, 11% recovery). MALDI-TOF-MS (monoisotopic) calcd for $C_{76}H_{91}N_{26}O_{13}$ (M+H): 1575.7. Found: 1575.9.

ImImImPy-(R)^{H2N}γ-PyPyPyPy-β-To-DACA (4)

Synthesized as described for **2** using *N*-(2-(dimethylamino)ethyl)-9-chloroacridine-4-carboxamide (0.5M, 3 μL) in DMF followed by the addition of 20 μL of DIEA (0.45 mg, 14% recovery). MALDI-TOF-MS (monoisotopic) calcd for $C_{80}H_{99}N_{26}O_{14}$ (M+H): 1647.8. Found: 1647.9.

ImImImPy-(R)^{H2N}γ-PyPyPyPy-β-Do (5a)

A sample of ImImImPy-(*R*)^{NHFmoc}γ-PyPyPyPy-β-Pam-resin (100 mg, 0.356 mmol/g) was suspended in 2,2'-(ethylenedioxy)bis(ethylamine) and heated at 55^{o}C for 12 h. The reaction mixture was filtered to remove resin, 0.1% (wt/v) TFA added (6 mL), and the resulting solution purified by reversed-phase HPLC. ImImImPy-(R)^{H2N}γ-PyPyPyPy-β-Do **(5a)** was recovered upon lyophilization of the appropriate fractions as a yellow powder (12 mg, 24% recovery). MALDI-TOF-MS (monoisotopic) calcd for $C_{67}H_{90}N_{23}O_{15}$ (M+H): 1284.6. Found: 1284.9.

ImImImPy-(R)^{H2N}γ-PyPyPyPy-β-To (5b)

Synthesized as described for **5a** using 4,7,10-trioxa-1,13-tridecanediamine (2 mL) for polyamide cleavage from resin (9 mg, 18% recovery). MALDI-TOF-MS (monoisotopic) calcd for $C_{67}H_{90}N_{23}O_{15}$ (M+H): 1356.6. Found: 1356.8.

ImImImPy-(R)^{H2N}γ-PyPyPyPy-β-Dp (5c)

Synthesized as described for **5a** using neat *N,N'*-(dimethylamino)propylamine (2 mL) for polyamide cleavage from resin (22 mg, 46% recovery). MALDI-TOF-MS (monoisotopic) calcd for $C_{57}H_{72}N_{23}O_{10}$ (M+H): 1238.6. Found: 1238.6.

ImImImPy-(R)^{NHBoc}γ-PyPyPyPy-β-Do (6a)

ImImImPy-(*R*)^{NHFmoc}γ-PyPyPyPy-β-Pam-resin was generated from Boc-β-alanine Pam resin (1 g, 0.59 mmol/g) using previously described Boc-protected monomers and methods.[45] A sample of the above polyamide on dried resin (200 mg, 0.356 mmol/g) was suspended in 4 mL of 4:1 piperidine-DMF and agitated (22^{o}C, 30 min). The resultant ImImImPy-(*R*)^{H2N}γ-PyPyPyPy-β-Pam-resin was washed sequentially with DCM and DMF. The resin was then suspended in 4 mL of NMP to which was added 500 mg of Boc_2O followed by 1 mL of DIEA, and the mixture was agitated (55^{o}C, 30 min). The resultant ImImImPy-(*R*)^{NHBoc}γ-PyPyPyPy-β-Pam-resin was washed sequentially with DMF, DCM, MeOH, and ethyl ether, and the amine-resin was dried in vacuo. A sample of resin was then treated with neat 2,2'-(ethylenedioxy)bis(ethylamine) (2 mL) and heated (55^{o}C) with periodic agitation for 16 h. The reaction mixture was filtered to remove resin, 0.1% (wt/v) TFA added (6 mL), and the resulting solution purified by reversed-phase HPLC. ImImImPy-(*R*)^{NHBoc}γ-PyPyPyPy-β-Do (**6a**) was recovered upon lyophilization of

the appropriate fractions as an off-white powder (24 mg, 23% recovery). MALDI-TOF-MS (monoisotopic) calcd for $C_{63}H_{82}N_{23}O_{14}$ (M+H): 1384.6. Found: 1385.0.

ImImImPy-(R)^{NHBoc}γ-PyPyPyPy-β-To (6b)

Synthesized as described for **6a** using neat 4,7,10-trioxa-1,13-tridecanediamine (2 mL) for polyamide cleavage from resin (32 mg, 31% recovery). MALDI-TOF-MS (monoisotopic) calcd for $C_{67}H_{90}N_{23}O_{15}$ (M+H): 1456.7. Found: 1457.3.

ImImImPy-(R)^{NHPEG2NH2}γ-PyPyPyPy-β-Dp (7)

A sample of ImImImPy-(*R*)^{NHFmoc}γ-PyPyPyPy-β-Pam-resin (200 mg, 0.356 mmol/g) was suspended in 4 mL of 4:1 piperidine-DMF and agitated (22°C, 30 min). The resultant ImImImPy-(*R*)^{H2N}γ-PyPyPyPy-β-Pam-resin was washed sequentially with DCM and DMF. The resin was then suspended in 4 mL of NMP to which was added 385 mg of Fmoc-8-Amino-3,6-Dioxaoctonoic acid preactivated with 360 mg HBTU and 0.5 mL of DIEA, and the mixture was agitated (55°C, 30 min). The resultant ImImImPy-(*R*)^{NHPEG2NHFmoc}γ-PyPyPyPy-β-Pam-resin was washed sequentially with DMF, DCM, MeOH, and ethyl ether, and the amine-resin was dried in vacuo. A sample of resin was then treated with neat 2,2'-(ethylenedioxy)bis(ethylamine) (2 mL) and heated (55°C) with periodic agitation for 16 h. The reaction mixture was filtered to remove resin, 0.1% (wt/v) TFA added (6 mL), and the resulting solution purified by reversed-phase HPLC. ImImImPy-(R)^{NHPEG2NH2}γ-PyPyPyPy-β-Dp (**7**) (4.7 μmol, 18%) was recovered upon lyophilization of the appropriate fractions as an off-white powder. MALDI-TOF-MS (monoisotopic) calcd for $C_{63}H_{82}N_{24}O_{13}$ (M+H): 1383.7. Found: 1383.9.

ImImImPy-(R)^{NHPEG2NHAcr}γ-PyPyPyPy-β-Dp (8)

Synthesized as described for **1** using 1 μmol **7**. (200 nmol, 20% recovery). MALDI-TOF-MS (monoisotopic) calcd for $C_{76}H_{89}N_{25}O_{13}$ (M+H): 1560.7. Found: 1560.9.

ImImImPy-(R)$^{NHC6\text{-}FAM}$$\gamma$-PyPyPyPy-Do-Acr (9)

ImImImPy-(R)^{NH2}γ-PyPyPyPy-Do-Acr was prepared as described for compound **1**, using Kaiser-oxime resin without β-alanine.[62] To 1 μmol of this compound dissolved in 100 μmol DMF was added 6-(fluorescein-5-carboxamido)hexanoic acid, succinimidyl ester (5-SFX, Molecular Probes, 10 μL, 0.1M in DMF), 10 μmol DIEA and the reaction was allowed to proceed at room temperature for 30 min. The mixture was then diluted with 0.1% (wt/v) TFA (8 mL) and the resulting solution purified by reversed-phase HPLC. Lyophilization provided ImImImPy-(R)$^{NHC6\text{-}FAM}$$\gamma$-PyPyPyPy-Do-Acr (**9**) as a yellow powder (550 nmol, 55% recovery). MALDI-TOF-MS (monoisotopic) calcd for $C_{95}H_{95}N_{24}O_{18}$ (M+H): 1862.0. Found: 1862.8.

ImImImPy-(R)$^{NHC6\text{-}FAM}$$\gamma$-PyPyPyPy-$\beta$-Do-Acr (10)

Prepared as described for **9** using 1 μmol **1**. (315 nmol, 31% recovery). MALDI-TOF-MS (monoisotopic) calcd for $C_{98}H_{100}N_{25}O_{19}$ (M+H): 1933.0. Found: 1933.6.

ImImImPy-(R)$^{NHC3\text{-}Bodipy}$$\gamma$-PyPyPyPy-$\beta$-Do-Acr (11)

1 μmol **1** was dissolved in 100 μmol DMF. To this was added 4,4-difluoro-5,7-dimethyl-4-bora-3a,4a-diaza-*s*-indacene-3-propionic acid (Molecular Probes, 10 μL, 0.1M in DMF), 0.9 μmol HBTU (1M in DMF), 10 μmol DIEA and the reaction was allowed to proceed at room temperature for 30 min. The mixture was then diluted with

0.1% (wt/v) TFA (8 mL) and the resulting solution purified by reversed-phase HPLC. Lyophilization provided ImImImPy-(R)$^{NHC3\text{-}Bodipy}$-γ-PyPyPyPy-β-Do-Acr (**11**) as a yellow powder (200 nmol, 20% recovery). MALDI-TOF-MS (monoisotopic) calcd for $C_{85}H_{93}BF_2N_{26}O_{13}$ (M+H): 1636.6. Found: 1736.2.

ImPyPyIm-γ-PyImPyPy-β-Do-AO (12)

ImPyPyIm-γ-PyImPyPy-β-Do (1 μmol aliquot) was added to 10 μL of phenol and dissolved by heating to 100°C. To this solution was added 4 μmol 9-methylthiooacridine dissolved in 5 μL DMSO, followed by 5 μL of DIEA, and the reaction was allowed to proceed at 100°C for 1 h. The mixture was then cooled to room temperature, diluted with 0.1% (wt/v) TFA (8 mL), and the resulting solution purified by reversed-phase HPLC. Lyophilization provided ImPyPyIm-γ-PyImPyPy-β-Do-AO (**12**) as a yellow powder (480 nmol, 48% recovery). MALDI-TOF-MS (monoisotopic) calcd for $C_{75}H_{89}N_{25}O_{12}$ (M+H): 1533.7. Found: 1533.6.

ImPyPyPy-γ-ImPyPyPy-β-Do-AO (13)

Synthesized as described for **12** using the ImPyPyPy-γ-ImPyPyPy-β-Do precursor (100 nmol, 10% recovery). MALDI-TOF-MS (monoisotopic) calcd for $C_{76}H_{90}N_{24}O_{12}$ (M+H): 1532.7. Found: 1532.7.

ImImImPy-γ-PyPyPyPy-β-Do-AO (14)

Synthesized as described for **12** using the ImImImPy-γ-PyPyPyPy-β-Do precursor (110 nmol, 11% recovery). MALDI-TOF-MS (monoisotopic) calcd for $C_{75}H_{89}N_{25}O_{12}$ (M+H): 1533.7. Found: 1533.7.

Construction of Plasmid DNA

The plasmid **pEF10** was constructed by insertion of the following hybridized inserts into the *Bam*HI/*Hin*DIII polycloning sites in pUC19: 5'-GATCC GGTAT ATATA GGGTA CGGAC CTATA TATAG GCTAT GTAGC GCGTA GGGTA TGTAG CGCGT AGGCT AC-3' and 5'-AGCTG TAGCC TACGC GCTAC ATACC CTACG CGCTA CATAG CCTAT ATATA GGTCC GTACC CTATA TATAC CG-3'. The insert was obtained by annealing complementary *Hind* III restriction fragments of pUC19 using T4 DNA ligase. The ligated plasmid was then used to transform JM109 subcompetent cells (Promega). Colonies were selected for α-complementation on 25 mL Luria-Bertani agar plates containing 50 mg/mL ampicillin. Cells were harvested after overnight growth at 37^{o}C. Large-scale plasmid purification was performed using WizardPlus Midi Preps from Promega. The presence of the desired insert was determined by dideoxy sequencing.

Preparation of 5'-End-Labeled Fragments

Two 21 base-pair primer oligonucleotides, 5'-GAATT CGAGC TCGGT ACCCG G-3' (forward) and 5'-TGGCA CGACA GGTTT CCCGA C-3' (reverse) were constructed for PCR amplification. The forward primer was radiolabeled using [γ-^{32}P]-dATP and polynucleotide kinase followed by purification using MicroSpin G-50 columns. The desired DNA segment was amplified as previously described.[63] The labeled fragment was loaded onto a 7% nondenaturing preparatory polyacrylamide gel (5% cross-link), and the desired 276 base-pair band was visualized by autoradiography and isolated. Chemical sequencing reactions were performed according to published protocols.[64,65]

Quantitative DNase I Footprint Titrations

All reactions were carried out in a volume of 400 μL according to published protocols.[63] Quantitation by storage phosphor autoradiography and determination of equilibrium association constants were as previously described.[63]

MPE·FeII Footprinting

All reactions were carried out in a volume of 400 μL according to published protocols.[63]

GCN4 Gel Mobility Shift Assay

Radiolabeled synthetic duplex DNA was prepared for gel mobility shift assay by treating with Sequenase (version 2.0), [α-^{32}P]-thymidine-5'-triphosphate and [α-^{32}P]-deoxyadenosine-5'-triphosphate for 3'-end labeling. The labeled duplex was purified using ProbeQuant G-50 Micro Columns. Polyamide was incubated with the duplex (20,000 cpm) in 40 μL reaction volumes of bisTris (10 mM, pH 7.0), NaCl (100 mM), DTT (1 mM), EDTA (1 mM), and poly(dI-dC)·poly(dI-dC) (5 μg/mL) for 16 h at 22^{o}C. GCN4 (222-281) was added and equilibrated for 45 min. Loading buffer (15% Ficoll, 0.025% bromophenol blue, 10 μL) was added, and 10 μL was immediately loaded onto a running 8% (29:1 acrylamide:bis-acrylamide) polyacrylamide gel (0.5 · TBE, 280 V, 0.8 mm, 13 cm). Separation of uncomplexed DNA and DNA-GCN4 (222-281) complexes was achieved within 40 min. Gels were dried in vacuo at 80^{o}C and then exposed to a storage phosphor screen (Molecular Dynamics).[66]

Sp1/Sp3 Gel Mobility Shift Assay

Radiolabeled synthetic duplex DNA was prepared as stated above and used as described with an Sp1/Sp3 gelshift kit purchased from Active Motif.

Unwinding Angle and Intrinsic Association Constant Determination

Relaxation reactions and numeric analyses were all carried out as described.[43,44] Minor variations to published protocols include two-dimensional gel electrophoresis carried out in 18 × 20 cm 1% agarose casting units and imaged after ethidium bromide staining with a Typhoon 8600 variable mode imager and 610-nm band-pass filter. The Boltzman distribution of adopted integer Lk values were plotted using equation (1),

$$I = I_M e^{[-w(\Delta Lk - \Delta Lk_c)^2]} \quad , \qquad (1)$$

where ΔLk and ΔLk_c are the measured linking difference and most abundant linking difference, respectively, I and I_M are integrated and maximum band intensity, respectively, and w is the distribution width. The apparent unwinding angle was calculated using equation (2),

$$\phi_{ap} = \frac{360 N_D(\Delta Lk_c - \Delta Lk^o_c)}{N_L} \quad , \qquad (2)$$

where ΔLk^o_c is the most abundant linking difference for the control reactions containing no polyamide, and N_D and N_L are the number of pUC19 and polyamide conjugate molecules, respectively. The actual unwinding angle was calculated using equation (3),

$$\phi_{ap} = \phi - \frac{\phi_{ap}}{K_a[C_N - (2n - 1)C_T]} \quad , \qquad (3)$$

where n represents the number of binding sites covered by one conjugate (set to unity), and C_N and C_T represent the concentration of conjugate binding sites and the concentration of polyamide conjugate, respectively. The C_N value was approximated

from 268 conjugate binding sites (and single base-pair mismatch sites) per ccDNA molecule for both **1** and **4**. The value of C_N affects the slope in Figure 2.7c but does not influence the value of ϕ (ϕ is the ordinate intercept).

Topoisomerase II Inhibition Assay

Topoisomerase II inhibition was tested as described from the Topogen Topo II drug screen kit. Briefly, varying concentration of polyamide were equilibrated with 10x topoisomerase II buffer and pBR22 overnight before treating with 4 units topoisomerase II (p170) for 30 min at 37^{o}C. The reaction mixture was then treated with 10% SDS and proteinase K to digest any ligated topo II enzyme prior to extraction with chloroform:isoamyl alcohol. The sample was then loaded directly onto a 1% agarose gel containing 0.5 mg/mL EtBr and destained before imaging.

In vitro Transcription

In vitro transcription run-off experiments were conducted on a *Hind*III restricted pBCKS+ plasmid as previously described.[52]

Confocal Microscopy

All cellular uptake experiments were completed by Benjamin S. Edelson as published.[53,54] Briefly, adherent cell lines were trypsinized for 5–10 min at 37°C, centrifuged for 5 min at 5°C at 2,000 rpm in a Beckman-Coulter Allegra 6R centrifuge, and resuspended in fresh medium to a concentration of 1.25 x 10^6 cells per mL. Suspended cell lines were centrifuged and resuspended in fresh medium to the same concentration. Incubations were performed by adding 150 µl of cells into culture dishes equipped with glass bottoms for direct imaging (MatTek, Loveland, OH). Adherent cells

were grown in the glass-bottom culture dishes for 24 h. The medium was then removed and replaced with 142.5 μl of fresh medium. Then 7.5 μl of the 100 μM polyamide solution was added and the cells were incubated in a 5% CO_2 atmosphere at 37°C for 10–14 h. Suspended cell line samples were prepared in a similar fashion, omitting trypsinization. These samples were then incubated as above for 10–14 h. Imaging was performed with a x40 oil-immersion objective lens on a Zeiss LSM 510 META NLO laser scanning microscope with a Coherent Chameleon 2-photon laser or on a Zeiss LSM 5 Pascal inverted laser scanning microscope.

Acknowledgment

We are grateful to the National Institute of Health (Grant 27681) for research support and a Research Service Award to E.J.F. We also thank the Ralph M. Parsons Foundation for a predoctoral fellowship to E.J.F.

References

1. Dervan, P. B., *Bioorg. Med. Chem.* **2001**, *9*, 2215-2235.
2. Gottesfeld, J. M., J. M. Turner, and P. B. Dervan, *Gene Expression* **2000**, *9*, 77-91.
3. Nielsen, P. E. *Curr. Med. Chem.* **2001**, *8*, 545-550.
4. Giovannangeli, C. and C. Hélène, *Curr. Opin. Mol. Ther.* **2000**, *2*, 288-296.
5. Pandolfi, P. P., *Oncogene* **2001**, *20*, 3116-3127.
6. Darnell, J. E., *Nat. Rev.-Cancer* **2002**, *2*, 740-749.
7. Kim, J. L., D. B. Nikolov, and S. K. Burley, *Nature* **1993**, *365*, 520-527.
8. Kim, Y. C., J. H. Geiger, S. Hahn, and P. B. Sigler, *Nature* **1993**, *365*, 512-520.
9. Pavletich, N. P. and C. O. Pabo, *Science* **1991**, *252*, 809-817.
10. Ellenberger, T. E., C. J. Brandl, K, Struhl, and S. C. Harrison, *Cell* **1992**, *71*, 1223-1237.
11. Keller, W., P. Konig, and T. J. Richmond, *J. Mol. Biol.* **1995**, *254*, 657-667.
12. Garvie, C. W., J. Hagman, and C. Wolberger, *Mol. Cell.* **2001**, *8*, 1267-1276.
13. Love, J. J., X. A. Li, D. A. Case, K. Giese, R. Grosschedl, and P. E. Wright, *Nature* **1995**, *376*, 791-795.
14. Lang, D. and T. Stamminger, *Nucleic Acids Res.* **1994**, *22*, 3331-3338.
15. Chen, F. E., D. B. Huang, Y. Q. Chen, and G. Ghosh, *Nature* **1998**, *391*, 410-413.
16. Ferredamare, A. R., G. C. Prendergast, E. B. Ziff, and S. K. Burley, *Nature* **1993**, *363*, 38-45.
17. Neely, L., J. W. Trauger, E. E. Baird, P. B. Dervan, and J. M. Gottesfeld, *J. Mol. Biol.* **1997**, *274*, 439-445.

18. Dickinson, L. A., R. J. Gulizia, J. W. Trauger, E. E. Baird, D. E. Mosier, J. M. Gottesfeld, and P. B. Dervan, *Proc. Natl. Acad. Sci.USA* **1998**, *95*, 12890-12895.

19. McBryant, S. J., E. E. Baird, J. W. Trauger, P. B. Dervan, and J. M. Gottesfeld, *J. Mol. Biol.* **1999**, *286*, 973-981.

20. Ehley, J. A., C. Melander, D. Herman, E. E. Baird, H. A. Ferguson, J. A. Goodrich, P. B. Dervan, and J. M. Gottesfeld, *Mol. Cell. Biol.* **2002**, *22*, 1723-1733.

21. Dickinson, L. A., J. W. Trauger, E. E. Baird, P. Ghazal, P. B. Dervan, and J. M. Gottesfeld, *Biochemistry* **1999**, *38*, 10801-10807.

22. Lenzmeier, B. A., E. E. Baird, P. B. Dervan, and J. K. Nyborg, *J. Mol. Biol.* **1999**, *291*, 731-744.

23. Wurtz, N. R., J. L. Pomerantz, D. Baltimore, and P. B. Dervan, *Biochemistry* **2002**, *41*, 7604-7609.

24. Dickinson, L. A., J. W. Trauger, E. E. Baird, P. B. Dervan, B. J. Graves, and J. M. Gottesfeld, *J. Biol. Chem.* **1999**, *274*, 12765-12773.

25. Winston, R. L., J. A. Ehley, E. E. Baird, P. B. Dervan, and J. M. Gottesfeld, *Biochemistry* **2000**, *39*, 9092-9098.

26. Oakley, M. G., M. Mrksich, and P. B. Dervan, *Biochemistry* **1992**, *31*, 10969-10975.

27. Oakley, M. G. and P. B. Dervan, *Science* **1990**, *248*, 847-850.

28. Kielkopf, C. L., S. White, J. W. Szewczyk, J. M. Turner, E. E. Baird, P. B. Dervan, and D. C. Rees, *Science* **1998**, *282*, 111-115.

29. Kielkopf, C. L., E. E. Baird, P. B. Dervan, and D. C. Rees, *Nat. Struct. Biol.* **1998**, *5*, 104-109.

30. Bremer, R. E., E. E. Baird, and P. B. Dervan, *Chem. Biol.* **1998**, *5*, 119-133.

31. Bremer, R. E., N. R. Wurtz, J. W. Szewczyk, and P. B. Dervan, *Bioorg. Med. Chem.* **2001**, *9*, 2093-2103.

32. See also: (a) White, C. M., A. L. Satz, T. C. Bruice, and T. A. Beerman, *Proc. Natl. Acad. Sci.USA* **2001**, *98*, 10590-10595. (b) He, G. X., K. A. Browne, J. C. Groppe, A. Blasko, H. Y. Mei, and T. C. Bruice, *J. Am. Chem. Soc.* **1993**, *115*, 7061-7071. (c) Browne, K. A., G. X. He, and T. C. Bruice, *J. Am. Chem. Soc.* **1993**, *115*, 7072-7079.

33. Lerman, L. S., *J. Mol. Biol.* **1961**, *3*, 18-30.

34. Denny, W. A., *Anti-Cancer Drug Des.* **1989**, *4*, 241-263.

35. Baguley, B. C., *Anti-Cancer Drug Des.* **1991**, *6*, 1-35.

36. Wang, A. H. J., *Curr. Opin. Struct. Biol.* **1992**, *2*, 361-368.

37. Gale, E. F., E. Cundliffe, P. E. Reynolds, M. H. Richmond, and M. J. Waring, *The Molecular Basis of Antibiotic Action*, 2nd ed.; John Wiley & Sons: New York, 1981.

38. Sakore, T. D., B. S. Reddy, and H. M. Sobell, *J. Mol. Biol.* **1979**, *135*, 763-785.

39. Crenshaw, J. M., D. E. Graves, and W. A. Denny, *Biochemistry* **1995**, *34*, 13682-13687.

40. Todd, A. K., A. Adams, J. H. Thorpe, W. A. Denny, L. P. G. Wakelin, and C. J. Cardin, *J. Med. Chem.* **1999**, *42*, 536-540.

41. Atwell, G. J., B. F. Cain, B. C. Baguley, G. J. Finlay, and W. A. Denny, *J. Med. Chem.* **1984**, *27*, 1481-1485.

42. Denny, W. A., G. J. Atwell, G. W. Rewcastle, and B. C. Baguley, *J. Med. Chem*. **1987**, *30*, 658-663.

43. Zeman, S. M., K. M. Depew, S. J. Danishefsky, and D. M. Crothers, *Proc. Natl. Acad. Sci.USA* **1998**, *95*, 4327-4332.

44. Zeman, S. M. and D. M. Crothers, *Methods Enzymol.* **2001**, *340*, 51-68.

45. Baird, E. E. and P. B. Dervan, *J. Am. Chem. Soc.* **1996**, *118*, 6141-6146.

46. All relaxation reactions were run at a sufficiently high (and constant) binding site-to-polyamide ratio to ensure that unwinding effects were only caused by sequence-specific interactions.

47. The 60 amino acid sequence (222-281) of GCN4 contains the 'leucine zipper' dimerization domain and the 'basic region' responsible for DNA binding.

48. The effects of polyamide-acridine conjugates binding only to the upstream site showed similar GCN4 inhibition values as ARE-41.

49. Suske, G., *Gene*, **1999**, 238, 291-300.

50. Miller et al., *J. Biol. Chem*. **1981**, 256, 9334-9339.

51. Capranico, G., S. Tinelli, F. Zunino, K. Kohn, and Y. Pommier, Y. *Biochemistry*, 1993, 32, 145-152.

52. Larsen, H. J. and P. E. Nielson, *Nucl. Acids Res.* **1996**, 24, 458-463.

53. Best, T. P., B. S. Edelson, N. G. Nickols, and P. B. Dervan, *Proc. Natl. Acad. Sci. USA* **2003**, 100, 12063.

54. Edelson, B. S., T. P. Best, B. Olenyuk, N. G. Nickols, R. Doss, S. Foister, A. Heckel, and P. B. Dervan, *Nucl. Acids Res.* **2004**, 32, 2802.

55. Bustamante, C., *Annu. Rev. Biophys. Biophys. Chem.* **1991**, 20, 415-446.

56. Muller, W. and D. M. Crothers, *J. Mol Biol.* **1968**, *35*, 251-290.

57. Waring, M. J. and L. P. G. Wakelin, *Nature* **1974**, *252*, 653-657.

58. Wang, A. H. J., G. Ughetto, G. J. Quigley, T. Hakoshima, G. A. van der Marel, J. H. van Boom, and A. Rich, *Science* **1984**, *225*, 1115-1121.

59. Dervan, P. B., *Science* **1986**, *232*, 464-471.

60. Bailly, C. and J. P. Henichart, *Bioconjugate Chem.* **1991**, *2*, 379-393.

61. Carrasco, C., P. Helissey, M. Haroun, B. Baldeyrou, A. Lansiaux, P. Colson, C. Houssier, S. Giorgi-Renault, and C. Bailly, *ChemBio.Chem.* **2003**, *4*, 50-61.

62. Belitsky, J. M., D. H. Nguyen, N. R. Wurtz, and P. B. Dervan, *Bioorg. Med. Chem.* **2002**, 10, 2767-2774.

63. Trauger, J. W. and P. B. Dervan, *Methods Enzymol.* **2001**, *340*, 450-466.

64. Maxam, A. M. and W. S. Gilbert, *Methods Enzymol.* **1980**, *65*, 499-560.

65. Iverson, B. L. and P. B. Dervan, *Methods Enzymol.* **1996**, *15*, 7823-7830.

66. Johnston, R. F., S. C. Pickett, and D. L. Barker, *Electrophoresis* **1990**, *11*, 355-360.